2008

Flexible Screw Design for Bone Implant Application

Seule Kabir
Virginia Commonwealth University

School of Engineering
Virginia Commonwealth University

This is to certify that the thesis prepared by Seule Kabir entitled FLEXIBLE SCREW DESIGN FOR BONE IMPLANT APPLICATION has been approved by her committee as satisfactory completion of the thesis requirement for the degree of Master of Science.

Muammer Koç, Ph.D., Thesis Director, School of Engineering

Dr. Jennifer S. Wayne, Ph.D., School of Engineering

Dr. Jonathan E. Isaacs, M.D., School of Medicine

Mohamed Gad-el-Hak, Ph.D., Chair, Mechanical Engineering, School of Engineering

Rosalyn S. Hobson, Ph.D., Associate Dean of Graduate Studies, School of Engineering

Russell D. Jamison, Ph.D., Dean, School of Engineering

F. Douglas Boudinot, Ph.D., Dean, School of Graduate Studies

Date

FLEXIBLE SCREW DESIGN FOR BONE IMPLANT APPLICATION

A thesis submitted in partial fulfillment of the requirements of the degree of
Masters of Science at Virginia Commonwealth University

By
Seule Kabir
B.S. Virginia Commonwealth University, 2007

Director: Dr. Muammer Koç
Associate Professor
Mechanical Engineering
Virginia Commonwealth University

Virginia Commonwealth University
Richmond, Virginia
December 2008

Acknowledgement

Here I would like to take a moment to thank several people. With honor, I would like to thank Dr. Russell Jamison for giving me the opportunity to continue my graduate education. I would like to express the deepest gratitude to Dr. Muammer Koç for guiding me throughout this study. My deepest appreciation is for Dr. Jennifer Wayne, for her support, forethought and caring advice throughout my studies. I am also thankful to Dr. Jonathan Isaacs for his support and guidance; this work would have not been possible without his support. I appreciate all my friends from School of Engineering, especially Eren Billur, for the assistance given to me during my time at VCU. I would like to give my special thanks to my family, my mom, my brother, and my sister; their patient love enabled me to complete this work.

Table of Contents

Page

List of Tables

Page

List of Figures

Page

Abstract

FLEXIBLE SCREW DESIGN FOR BONE IMPLANT APPLICATION

By
Seule Kabir, M.S.

A thesis submitted in partial fulfillment of the requirements of the degree of
Masters of Science at Virginia Commonwealth University

Virginia Commonwealth University, 2008

Director: Dr. Muammer Koç
Associate Professor
Mechanical Engineering

Disruption of the scapholunate ligament can result in significant immediate and long-term disability. Of the available current acute and subacute treatment strategies for this disorder, the use of a solid screw to stabilize the scapholunate relationship has been proposed. However, subsequent carpal bone loss is an inherent risk to this technique. The goal of this study was to design a flexible orthopedic screw that can be placed between the scaphoid and lunate to restore more normal biomechanics without the risk of osteolysis.

Several ideas were generated during the course of the study to create a moveable section in a bone screw implant. Designs that met the specifications and were promising from the manufacturing point of view were tested using finite element analysis. Some designs were prototyped and one of them was tested using a cadaver wrist. Every design concept revealed some positive and negative features in terms of manufacturing and functionality. It is promising in terms of fulfilling the design requirements, but prototyping the design was very difficult. In conclusion, it can be said that the invented flexible screw techniques are sufficient to hold the scaphoid and lunate together after the scapholunate ligament injury, to restore more normal wrist biomechanics.

CHAPTER 1 BACKGROUND AND STATE OF THE ART

1.1 Introduction and Motivation

The wrist is a complex joint connecting the distal forearm to the hand with eight small bones and connecting ligaments. A balance among the bony surfaces and ligament restraints provides both mobility and stability in the wrist during normal activities (Jaruga et al, 2006). Disruption of any of the ligaments or bone ligament interfaces can result in significant immediate and long term disability. The resulting biomechanical or morphological changes in the wrist can lead to arthrosis, instability, chronic discomfort and loss of functional movement (Rosenwasser, Miyasajsa, and Strauch, 1997).

Of all the ligaments in the wrist, Scapholunate Interosseous (SLI) ligament is the cornerstone of normal wrist biomechanics. Disruption to this ligament, known as scapholunate dissociation or instability, causes the scaphoid to shift into an abnormal position. With time, the wrist collapses and at the final stage the collapse results in a predictable arthritic pattern referred to as a scapho-lunate advanced collapse or SLAC. The resulting anatomical changes not only cause pain but also diminish the normal functional mobility of the wrist for the patient.

There are several surgical techniques to treat scapholunate dissociation. One of them is to bridge the scaphoid and lunate with a rigid screw in an effort to establish a stable pseudoarthrosis between the two bones However, in this construct, a rigid screw is

placed between two moving bones creating a potential “windshield wiper” effect by loosening the screw which could result in catastrophic scaphoid or lunate bone loss. To overcome this significant drawback, a novel approach is proposed in this study to couple the scaphoid and lunate together in a flexible way. The motivation is to create a strong repair, and reduce the gap between scaphoid and lunate by implanting a flexible screw between the bones (Fig. 1). The hypothesis was that the mechanical coupling will correct short term instability problems while formation of a pseudoarthrosis between the scaphoid and lunate will prevent long term arthritic problems. Because of the flexibility of the system, the windshield wiper effect and subsequent bone damage would be avoided, and improved preservation of wrist motion and closer to normal wrist biomechanics is predicted.

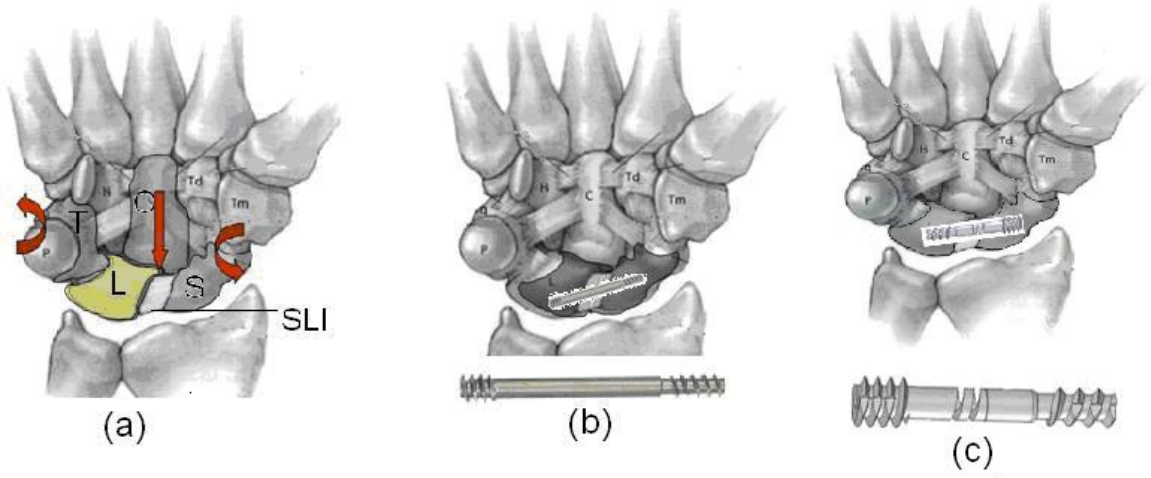

Figure 1: (a) Mechanism of injury showing the displacement direction of scaphoid (S) and triquetrum (T) and capitate (L) after injury to the SLI ligament. Under the normal condition these movements are balanced by the lunate (L) and intrinsic ligaments like SLI. (b) One of the current techniques of using solid screw to join the scaphoid and lunate. (c) Goal of the study to improve this technique to join scaphoid and lunate with a flexible screw. (Modified image from Doyle and Botte, 2003)

The application of flexible or movable link system to make orthopedic screws is unique with respect to all other technologies that are being used today. It allows several movements such as tension or compression, bending and rotation between the two bones and simplifies the surgery. Therefore, it is in some ways more effective and in others, more forgiving. Also, the system may have several other potential applications which further enhance the potential of this study.

This particular design does not have the disadvantages of current products on the market. However, there were certain challenges to confront during the course of the study. One of the challenges was prototyping; the cost to produce an exact product for a small amount of capital was difficult. If this can be overcome, it is believed that the flexible screw is sufficient to hold the scaphoid and lunate together so that the scaphoid does not sublux and more normal wrist biomechanics is restored.

Understanding normal and abnormal biomechanics of the wrist is the foundation of this study. The anatomy of the wrist must be comprehended for this. In this chapter, anatomy of the wrist is presented with detail on the scaphoid, the lunate and the SLI ligament, followed by the biomechanics and kinematics. Several design ideas that were generated during the course of study are presented in Chapter two. Chapter three details how these designs were tested and Chapter four, how they were compared in order to draw a conclusion.

1.2 Wrist Anatomy

The wrist is a complicated and unique joint interposed between the distal aspect of the forearm and the proximal aspect of the hand. It consists of the proximal end of the five metacarpal, carpal bones and the distal radius and ulna. The carpal bones are eight small bones, classically described as being in two rows. The scaphoid, lunate, triquetrum, and pisiform form the proximal carpal row, and trapezium, trapezoid, capitate, and hamate form the distal carpal row (Fig. 2). The elements are connected by extrinsic and intrinsic ligaments. The extrinsic ligaments, also known as radiocarpal and ulnocarpal ligaments, connect the proximal carpal row with the radius and ulna of the forearm. The intrinsic ligaments connect the eight carpal bones with each other. They allow a wide range of motion that is limited at the extremities and determined by the bone shape and ligamentous attachment (Cooney, 1998). The structure allows radial and ulnar deviation, flexion and extension, pronation and supination, and translation in three planes.

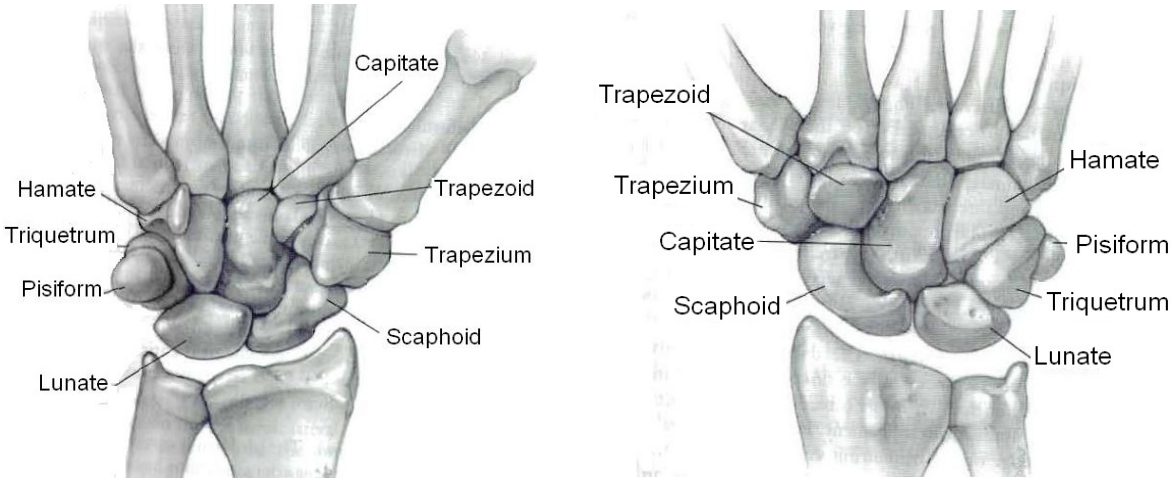

Figure 2: Palmar (left) and dorsal (right) view of the wrist showing the distal end of the radius and the ulna, the eight carpal bones, and the proximal end of the five metacarpals. (Modified image from Doyle and Botte, 2003)

The task of this study was to restore the normal biomechanics of the wrist by coupling the scaphoid and lunate in a flexible way in case of SLI injury. Therefore, the focus of the study was centered on the scaphoid, the lunate and the scapholunate interosseous ligament.

The scaphoid, articulating with four carpal bones and the radius, is the site of attachment for important ligaments and capsule. Approximately 80% of its entire surface is covered by four articular facets, articulating with scaphoid fossa of the distal radius, lateral aspect of the lunate, lateral aspect of the capitate, medial and lateral aspect of the trapezoid and trapezium respectively (Cooney, 1998). The scapholunate interosseous ligament (SLI) is attached at the proximal margin of the medial articular surface (Fig. 2).

In a study done by Heinzelmann, Archer, and Bindra, 30 paired cadaveric specimens were measured for scaphoid length and width. Male specimens were found to be significantly larger than the female ones. The average length was 31.3 mm for male and 27.3 mm for female. The proximal width was 4.4 mm for male and 3.7 mm (although this dimension seems small in comparison to anatomical images) for female specimens. Distal width was same for both male and female, 7.2 mm. The waist width was 13.6 mm for male and 11.1 mm for female specimens (Heinzelmann, Archer, and Bindra, 2007).

The lunate, also articulating with five bones, is considered the keystone of the carpus. From a study done by Gupta and Moosawi, using CT examination of fifty wrists, the mean maximum antero-dorsal diameter of the lunate measured on axial section was shown to be 16.96 mm with the range of 13–19 mm. The average medio-lateral diameter of the lunate was 12.80 mm with the range of 10–15 mm (Gupta and Moosawi, 2002).

Additionally, the lunate is larger palmarly than dorsally (Cooney, 1998). These dimensions provide constraints for the design and were considered in the design of the implant.

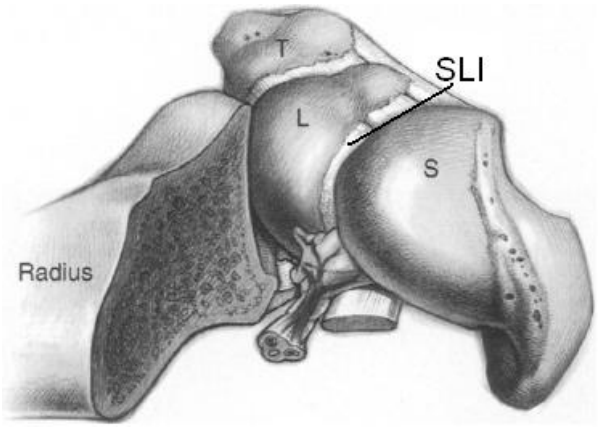

Figure 3: Radial and proximal drawing of the scapholunate interosseous (SLI) ligament forming a connection between the dorsal, proximal, and palmar regions of the scaphoid (S) and lunate (L). Lunate is also connected with the triquetrum (T) through ligaments. The radial styloid region is excised to have a proximal view of the SLI ligament. (Image modified from Berger, 1996)

Among the ligaments, the scapholunate interosseous ligament (SLI) is the cornerstone of normal wrist biomechanics (Fig. 3, 4). It is mostly described as a C shaped true ligament with collagen fiber organization in the dorsal to palmar region. The dorsal region of the ligament is relatively thick and composed of transversely oriented collagen fibers while the palmar region is quite thin. It is oriented obliquely in the transverse plane from lunate to scaphoid and thus allows various ranges of motion during different wrist movements (Doyle and Botte 2003). The thickness of the ligament varies from 2 to 3 mm and the length varies from 2 to 5 mm (Cooney, 1998). It is a complex structure that connects the scaphoid and lunate by their mutually articulating dorsal, proximal, and

palmar edges (Berger and Rochester, 1996). Details about the motion of these two bones are explained in Chapter two of Design Specifications for the implant.

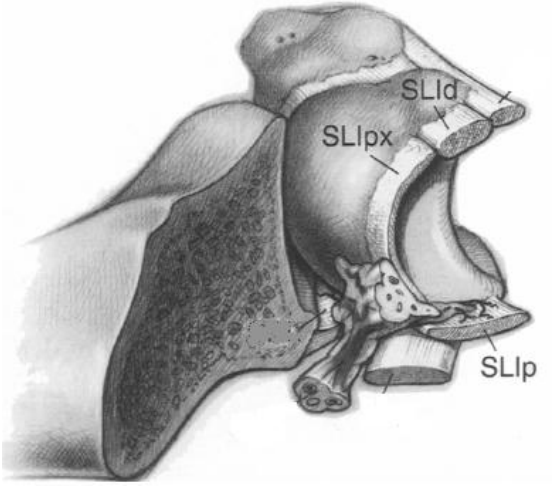

Figure 4: Drawing of the Scapholunate Interosseous (SLI) ligament, from a radial and proximal perspective with scaphoid removed. The image shows three regions of the ligament, the dorsal (SLId), the proximal (SLIpx) and the palmar (SLIp). (Modified image from Berger, 1996)

1.3 Kinematics and Biomechanics

Carpal kinematics is explained in terms of rows and columns in the literature but mostly in proximal and distal row kinematics (Craigen and Stanly, 1995). The two bones that are of interest, the scaphoid and lunate, are part of the proximal row with the triquetrum and pisiform. The SLI ligament is placed in the proximal region between the scaphoid and lunate, away from the axis of rotation between the bones, and thus provides rotational stability (Lichtman 1988).

A considerable amount of load is transmitted through the carpal bones during the daily activities using the upper arm. The loads are distributed not only on the articular

cartilage and ligaments but also to the joint architecture and tendons. Garcia-Elias stated that during grasping an object, the total force transmitted from the metacarpals to the distal carpal row is about ten times greater that the applied force at the tip of the finger (Garcia-Elias, 1996). About fifty percent of the load is transmitted from capitate to the scaphoid and lunate (Cooney 1998).

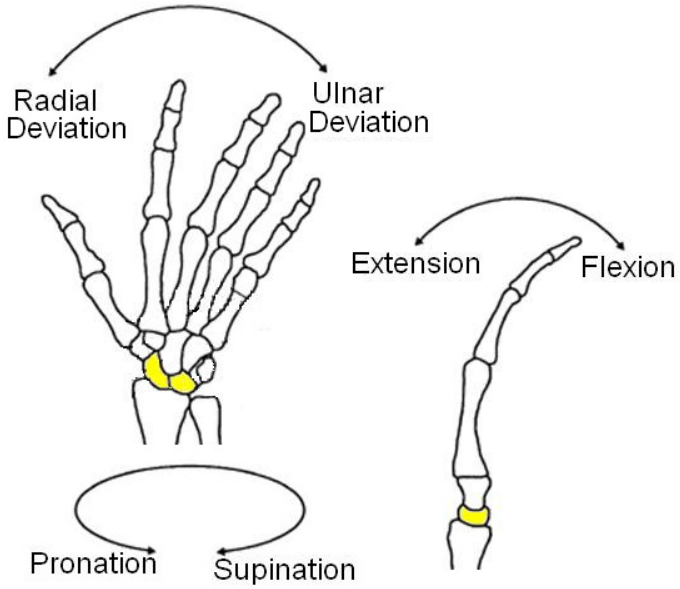

Figure 5: Movements of the wrist showing the direction of radial/ulnar deviation, flexion/extension, and pronation/supination by showing the left palmar view of the wrist and the hand. The scaphoid (left) and lunate (right) are highlighted on the left image and lunate is highlighted on the right image (Image modified from internet)

MacConaill, in 1941, proposed a subdivision of the carpus which singled out the scaphoid as an intercalated rod between the proximal and distal carpus (Julio 1985). Its complex motion can be interpreted from the orientation of ligaments and bones around it. The joint between the scaphoid and capitate are convexo-concave and is responsible for the

complex mobility of the scaphoid. With the radius it has not only rolling but also some sliding motion, the radio-scaphocapitate ligament prevents it from pure flexion and extension. On average the scaphoid extends about 50º and flexes about 58º, supinates about 6º and deviates about 4º in radial direction from start to finish (Cooney 1998).

The lunate extends about 38º, pronates 5º and deviates 3º when the wrist moves from the neutral position. During radial deviation, the lunate flexes about 11º, radially deviates about 8.6º and pronates about 6º. During ulnar deviation of the wrist, the lunate extends 32º, ulnarly deviates about 16º and supinates about 5º (Cooney 1998). These motions are shown in Figure 5. More about the relative angular movements of these two bones are explained in Chapter two.

So it can be said that considerable multiplanar motion occurs between the scaphoid and lunate with triquetrum at the interosseous joints. While the scaphoid is flexing and the triquetrum extending during hand positioning, intrinsic ligaments connects these two bones via the lunate to keep the system in balance (Kuo and Wolfe, 2008). Alteration to this joint architecture results in abnormal transmission of force. For example, when the SLI ligament is disrupted, isolated subluxation (partial dislocation) of the scaphoid occurs. The lunate and triquetrum remain extended. If not treated, the scaphoid subluxes in to more painful position since there is no balancing force from lunate and triquetrum. With time this allows the capitate to push between the lunate and scaphoid, resulting in carpal collapse, termed as DISI, dorsal intercalated segment instability (Cooney 1996).

1.4 Injury to the Ligament

There are three terms used in literature related to SLI ligament injury; (1) scapholunate instability, (2) rotatory subluxation of the scaphoid, and (3) scapholunate disassociation. In some cases these terms were interchanged with (1) anatomical change, (2) radiographic alignment of disassociated scaphoid and (3) ligament tear, respectively. For simplicity, in this study scapholunate injury resulting in instability or disassociation is to be considered as an injury causing the patient to be unable to withstand loads applied to the bone ligament interface during daily activities, or unable to perform carpal motions.

In numerous publications, it is stated that scapholunate instability is the most frequent form of carpal instability and causes a considerable amount of dysfunction. Disruption of the ligaments or bone ligament interfaces results in significant, immediate and long term disability. The resulting biomechanical or morphological changes in the wrist can lead to arthrosis, instability, chronic discomfort and loss of functional movement (Rosenwasser, Strauch, and Miyasajsa, 1997). When this injury creates an unstable joint between scaphoid and lunate or changes the way the joint moves, the forces on the articular cartilage increase. Over the span of years, this imbalance in joint mechanics damages the articular cartilage. One of the problems with the articular cartilage is that it cannot heal itself well and the damage accumulates. As a result, the joint can no longer compensate for the damage.

Scapholunate instability is not only the disruption of the SLI ligament but a spectrum of injury. Different stages associated with the instability were described in literature as a progression of the injury. Along this spectrum, in addition to the SLI

ligament, other ligaments may fail. This can occur with increasing severity of the trauma or chronicity of the injury. The scaphoid and lunate fall into an abnormal posture including gapping between the bones once enough ligament failure occurs. This is known as scapholunate dissociation (Kuo and Wolfe, 2008). The resulting flexion of the scaphoid, extension of the lunate and triquetrum (known as DISI (Dorsal Intercalated Segment Instability)), allows migration of the capitate. The anatomical changes of these bones, scaphoid, capitate, and lunate, become irreversible as the ligaments and structures around them remodel (Kuo and Wolfe, 2008).

The resulting altered carpal kinematics progresses to abnormal articular loading, followed by an arthritic pattern referred to as a scapho-lunate advanced collapse (SLAC). This condition is irreversible and soft tissue reconstructive techniques are not enough to treat the injury. In the literature four stages of SLAC have been described. Stage I is the narrowing of the radioscaphoid joint at the radial styloid aspect. When this progresses to stage II, radioscaphoid joint collapses completely. This alters the normal load-bearing ability of the capitolunate joint. Resulting shear stress destroys cartilage in the capitolunate joint leading to stage III midcarpal scapholunate advanced collapse. As the arthritic pattern progresses it reache stage IV involving collapse of the entire carpus (Danikas and Dimitrios, 2005).

1.5 Repair techniques

The terms associated with the stage of injury and their suggestive treatments are very subjective in the literature. For example, Larsen defines acute as less than a week, subacute as one to six weeks and chronic as more than six weeks (Larsen, 1996). Baratz et al defined acute as less than three months (Baratz et al 2006). A thorough understanding of all these repair techniques was beyond the scope of this study. Therefore, the focus was narrowed to the principles of repair techniques when the gap between the scaphoid and lunate is reducible. Some of the repair techniques at the stage when the gap is reducible, includes direct ligament repair combined with dorsal capsulodosis, tenodesis, bone-ligament-bone technique, intercarpal fusions and RASL (re-approximation of scaphoid and lunate). As the injury progresses, more force is required by the system to keep the bones in place. Therefore, at the final stage of the injury spectrum, the only repair techniques involve intercarpal fusion.

Capsulodesis is recommended to prevent scaphoid flexion by attaching the scaphoid with another bone using a capsular flap. For example, in the Blatt capsulodesis technique (Fig. 6), a dorsally based capsule is attached to the radial styloid and the SL joint is reduced. This technique provides pain relief for the patient by preventing the scaphoid from being over flexed from a certain point, but does not completely resolve the problem. Since the lunate remains tilted, a radiograph after healing from the surgery shows abnormal positioning of the scaphoid and lunate, indicating that the procedure does not correct carpal malalignment and as a result the normal wrist kinematics is not restored (Moran et al, 2005

and Rosenwasser, Strauch, and Miyasajsa, 1997). The gap between the scaphoid and lunate is also not reduced in this technique.

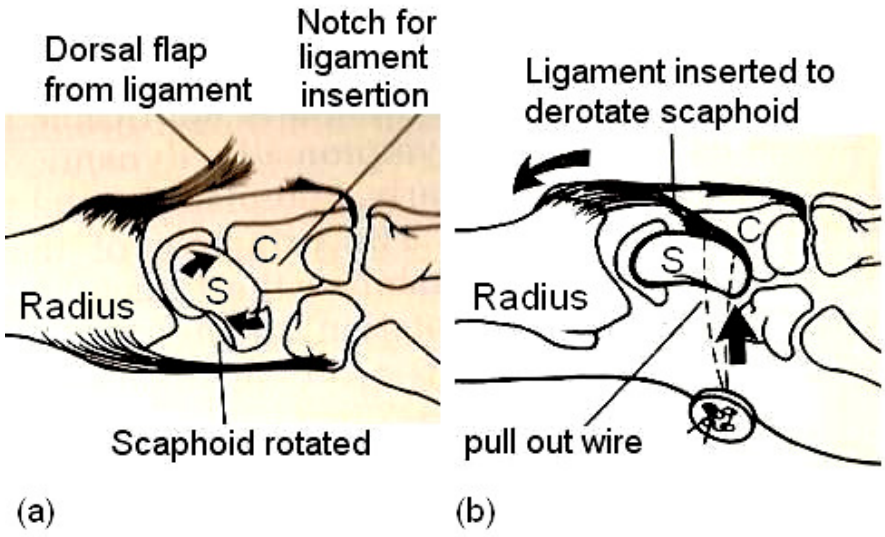

Figure 6: Blatt Dorsal Capsulodesis technique. (a) A distally based capsular flap is attached with the scaphoid (S). (b) Derotation of the scaphoid is created using the capsule. (Image modified from Litchman, 1988)

In tenodesis technique, a tendon is passed through the carpal bones to reduce the abnormal bone alignment. For example, in Brunelli tenodesis the tendon is passed through a drilled tunnel in the scaphoid and the remainder of the ligament is attached to the dorsal radius or lunate (Chabas 2008). The drawback of this technique is that the mechanical properties of the tendon are not similar to the ligament, and thus, can lead to abnormal positioning of the bones with pain in the wrist. Balancing the length of the tendon with the bony anatomy can also be challenging in an injured wrist (Baratz et al, 2006).

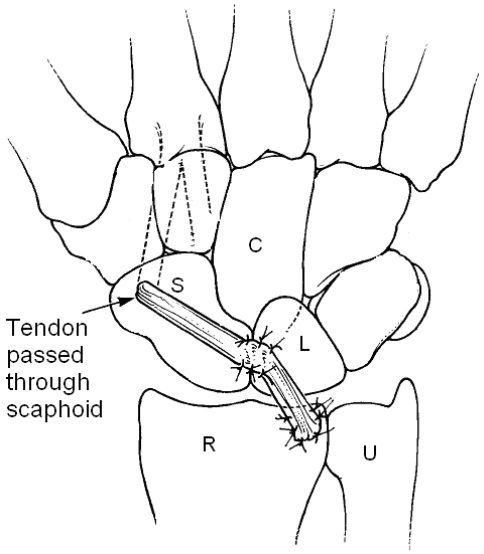

Figure 7: Tenodesis of scaphoid and lunate, tendon graft is passed through the scaphoid (S) and connecting to the lunate (L). It may also be connected to the radius (R). The ulna (U) and the capitate (C) is also shown (Image modified from Wolfe, 2001)

Bone-Tissue-Bone autograft (Fig. 8) is another technique used in reducible scapholunate instability when no ligament is left to repair. In this technique, a small bone tissue interface is harvested from the foot or wrist. From the dorsal proximal scaphoid and the radial lunate, a similar sized block of bone is removed and the harvested bone tissue interface is placed by transfixing the system with k-wire (also known as Kirschner wire, a smooth stainless steel pin with a drill tip. It is mainly used on orthopaedics for fixation of fracture and skeletal traction (Franssen, 2008)). Sometimes a Herbert screw is used which is taken out after one year of the surgery. This technique allows force to be transmitted through both the scaphoid and lunate. The drawback of this procedure is that significant long term changes in soft and bony tissue causes increased tension between the joints (Baratz et al., 2006). A combination of bone-tissue-bone technique with the Herbert screw

is reported to have success (Harvey, 2007) however, the patient then needs to visit the hospital for an additional surgery within a year period for the removal of the screw. This is also a very technically demanding procedure.

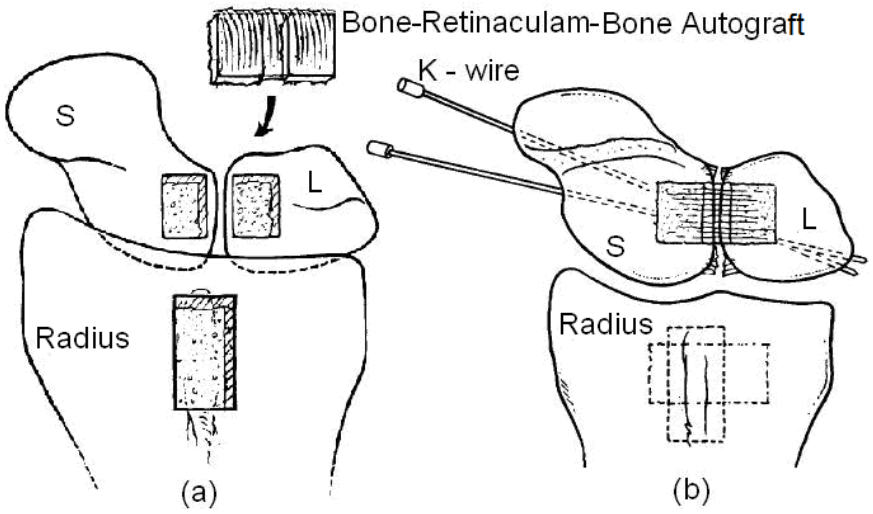

Figure 8: Bone-Tissue-Bone Technique. (a) Autograft from radius placed between the scaphoid (S) and the lunate (L), (b) The system is transfixed with K-Wire (Image modified from Weiss, 1998)

One of the problems with soft tissue reconstruction, such as capsulodesis, tenodesis or bone-ligament-bone technique, is the gapping force between the scaphoid and lunate. The bones tend to dissociate due to the changes in soft tissue or bony changes over time. To address this issue, Rosenwasser, Strauch, and Miyasajsa proposed a technique called RASL (re-approximation of scaphoid and lunate). The main idea of this technique is to join the scaphoid and lunate by forming a pseudo-arthrosis (stable scar tissue formation helps to maintain the reduced position). The procedure (Fig. 9) involves the roughening up and decorticating of the interval between the scaphoid and lunate to encourage the formation of

scar tissue. The bones are brought closer to each other with K-wires like a joysticks and kept in position by clamping the joysticks. A headless Herbert screw is placed beneath the bones at the axis of rotation using insertion instruments. The screw is used to hold the bones together long enough to allow the formation of scar tissue between the scaphoid and lunate. The ball of scar tissue referred to as a pseudo-arthrosis is supposed to hold the bones together to prevent collapse of the bones while allowing some motion between the bones (Rosenwasser, Strauch, and Miyasajsa, 1997).

There are several advantages to this technique compared to the others described earlier. It couples the bones tightly in a reliable way and the “pseudo-arthrosis” probably does add legitimate stability. Also no other carpal bone or ligament is altered in this technique so if any secondary reconstruction is needed in the wrist, it can be done. The problem with the procedure is significant, however. The procedure does not include a screw removable. So the fixed screw is assumed to be left between two moving bones. The consequence of this is that it may loosen over time, causing the screw to move back and forth. This is referred as “windshield wiper effect” and can cause significant bone destruction. In the case of the scaphoid or lunate bones, this type of destruction would be disastrous.

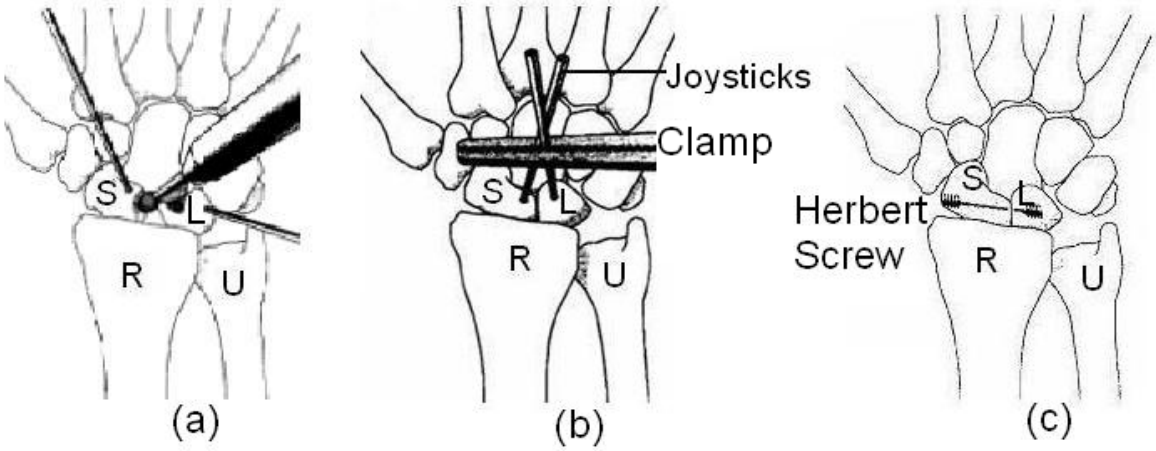

Figure 9: RASL Procedure. (a) Contact area between the scaphoid and lunate is roughened to encourage the formation of pseudo-arthrosis. (b) Use of joystick to reduce gap between scaphoid (S) and lunate (L). (c) Herbert screw is placed within the scaphoid and lunate at their axes of rotation (Modified image, Rosenwasser, Strauch, and Miyasajsa, 1997)

Keeping in mind the potential benefits and risks involved with the RASL technique, we hypothesized that a screw with a flexible system could be developed that can maintain the strong coupling achieved with RASL procedure, while avoiding some drawbacks.

1.6 Wrist Implants

There are several types of implants that are currently available and used in procedures similar to RASL. They all have some similar features and some unique features. However, most of them seem to be modified from Dr. Timothy Herbert's design, done in 1970s. The screw (Fig. 10) is available in the U.S. by Zimmer® (Warsaw, Indiana) with cannulation design modification done by Dr. Terry Whipple, former associate professor at the Medical College of Virginia. The screw is headless and thus can be placed

within the bone. The leading and trailing edges have different pitch lengths with wider trailing edge which keeps the bony area in compression.

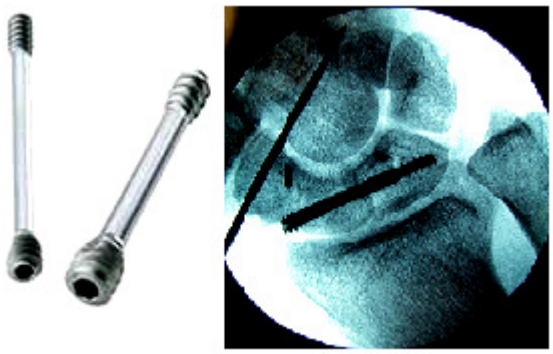

Figure 10: Herbert Whipple screw (Herbert/Whipple, 2008) and screw placement through scaphoid and lunate bone in SLI ligament injury (Budoff, 2008)

Orthosurgical Implant Inc. (Miami, Florida) has a very similar screw, the Herbert Bone Screw or HBS (Fig. 11), used to couple the scaphoid and lunate after SLI ligament injury (Aviles 2007). This screw is similar to the Herbert Whipple screw except it has a smaller shaft diameter and hexagonal screw head for insertion. The company claims that the new HBS screw has better compressibility than the Herbert screw.

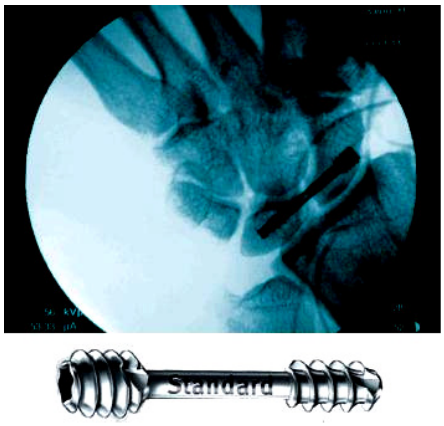

Figure 11: The new HBS screw (Modified image from the brochure of the screw, Orthosurgical 2008)

The TwinFix Cannulated Compression Screw from Stryker® (Freiberg, Germany) is another type of rigid screw (Fig. 12) that is used for the treatment of fractures and pseudarthroses of the scaphoid bone and fusion of the carpal bones. This screw has several unique features in comparison to the Herbert screw. The trailing edge has a separate section which can rotate independently relative to the rest of the screw body. This might be useful for intercarpal fusion technique, however, no documented literature has been found on this. Its self tapping technique is claimed to minimize the disruption of fracture site during insertion.

Figure 12: TwinFix Cannulated Compression Screw (Modified image from the brochure of the screw, Stryker 2008)

Although not found in any literature, some orthopaedists use the Acutrak screw from Acumed® (Hillsboro, Oregon) for the treatment from SLI ligament injury (Fig 13). This screw is also cannulated but headless, which allows it to be implanted below the surface of the bone. The concept of variable thread pitch is employed here for the same reason as the Herbert screw, but fully threaded. This feature may improve internal holding power with the continuous threads of different pitches, as well as allowing a fracture or osteotomy site to lie anywhere along the length of the screw.

Figure 13: Acutrak Screw (Acumed 2008)

A recently patented screw, the SLIC screw (Fig 14), is promising for the treatment of SLI ligament injury. It is a modification of the Acutrak having two parts connected with a ball and socket joint. The screw is cannulated and threaded on its entire length.

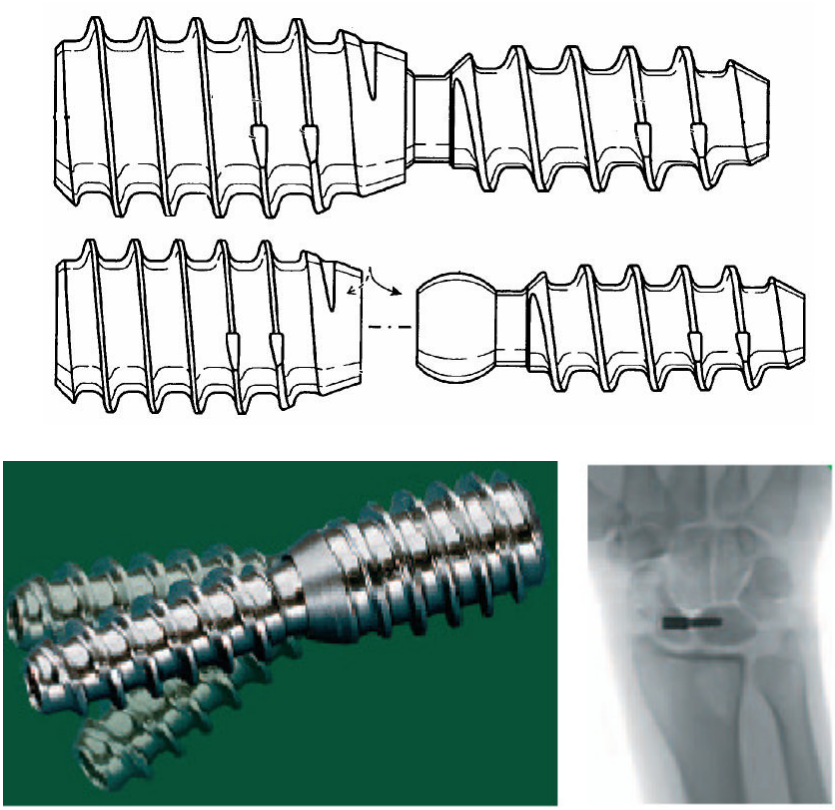

Figure 14: SLIC screw joining scaphoid and lunate. (Sucec and Tuller, 2006)

The SLIC screw, specific for the SLI ligament injury came in the market during the time this study was conducted. It has two parts connected with ball and socket joint between the leading and trailing screws to allow 360º of rotation. Therefore, when this screw is placed within the bone, the bones are able to move relative to each other. This design addresses the same problem investigated in this study with a similar approach as the study hypothesizes. However, the screw was in the market for a very short period of time and was removed abruptly except the patent which still exists.

We theorized that this rapid withdrawal from the market is due to failure of the system. The connection point of the screws may not be strong enough to hold the force

applied proximally by the capitate on the lunate and scaphoid. Another potential problem might be the manufacturing of such a small parts. All of these issues together can also lead to a short fatigue life even if it possible to manufacture and assemble.

All of the repair techniques explained in this chapter work in selected cases and they all suffer from unpredictability and loss of motion. One of the main obstacles is to reconstruct the coupling of the scaphoid and lunate in a reliable way to heal the injury, and maintain the scaphoid and lunate relative positions. Keeping positive and negative of all these techniques in mind, the goal was to approach a reliable solution to couple the scaphoid and lunate after injury using a flexible implant.

CHAPTER 2 DESIGN OF IMPLANTS

The implant designed in this study would be used to couple the scaphoid and lunate wrist bones in case of the SLI ligament injury. Therefore, this is an alternative to the existing wrist implants. In an article about *Design Consideration for a Wrist Implant*, Shepherd and Johnstone stated that the main design requirements of wrist implants are to relieve the resulting pain, stabilize the joint, and provide a functional range of motion and correct the deformity (Shepherd and Johnstone, 2002). These requirements are to be followed for any implant design. Keeping these in mind, a novel design approach was taken to couple the scaphoid and lunate together in a flexible way. In this chapter, design specifications, proposed designs, and issues related to research will be discussed.

2.1 Design Specifications

Design specifications were selected based on the anatomy of the wrist, literature study of the kinematics of the scaphoid and lunate, and state of the art review of the implants that are available in the market now. The specifications are described below:
(1) Degree of relative motion: During wrist motions, the scaphoid and lunate move significantly relatively to each other. Short and Werner have conducted several studies on the kinematics of the scaphoid and lunate joint. In one case (Short et al, 1997) they

reported that when the wrist extends 30º, the scaphoid extends approximately 20º. In the same position the lunate extends about 12º. During wrist 50º flexion, the scaphoid flexes about 35º and the lunate flexes about 25º. The relative motion between these two bones is about 8 to 10º. According to another study (Werner, Short and Green 2005), during maximum flexion of the wrist the scaphoid extends about 28.2º and the lunate extends about 17.6º for the same position. During maximum flexion the scaphoid flexes about 26º and lunate flexes about 18º. So the relative motion is also 10º to 8º. Litchman stated that scaphoid and lunate "bind the proximal row into a unit of rotational stability. Thus in radial and ulnar deviation the amount of intercarpal rotation allowed by the system is approximately 4º at the scapholunate joint. However in flexion and extension, there can be as much as 30º at the scapholunate joint" (Lichtman 1998). Julio stated that "from neutral to dorsiflexion, the lunate rotates approximately 28º and the scaphoid 30º. From neutral to complete volarflexion the lunate rotates 30º and the scaphoid 60º" (Julio 1985).

From these studies, it was understood that the maximum rotation between the bones, relative to each other, is maximum 30º. Therefore, for the design criteria, relative rotation of the leading edge and trailing edge was set to 30º maximum.

(2) Length of the Flexible section: Two factors, length of the ligament and distance between the scaphoid and lunate after SLI ligament injury, were considered to determine the length of the flexible section.

According to a series of studies on "Biomechanical evaluation of ligamentous stabilizers of the scaphoid and lunate" done by Short et al, the distance between scaphoid and lunate increases in different positions as different intrinsic and extrinsic ligaments are

injured or cut (Short et al, 2002, 2005, 2007). In an intact wrist, the distance between scaphoid and lunate is approximately1.6 mm in maximum flexion and 1.2 mm in maximum ulnar deviation. For this design the focus was on the distance between the bones after SLI ligament is injured. When only the SLI ligament is injured or cut the distance is 2.2mm. The length of the ligament is also varies from person to person and on average, it is from 2 to 5 millimeter.

This understanding set the second design criteria; the length of the flexible section between the leading and trailing screws, to be less than or equal to 5 mm.

(3) Total Length: To determine the total length, x-ray of the wrist was studied and suggested to be 20 mm by Dr. Jonathan Isaacs, one of the advisors in this study.

(4) Major Diameter and Shaft Diameter: The major diameter was set to be around 3.2 – 3.7 mm based on the x-ray study as well.

In summary, these are the design specifications that were accepted to follow at the outset of this study.

1. Degree of relative motion, 30º
2. Length of the flexible section $\leq$ 5 mm
3. Total length about 20 mm increment
4. Major diameter about 3 mm

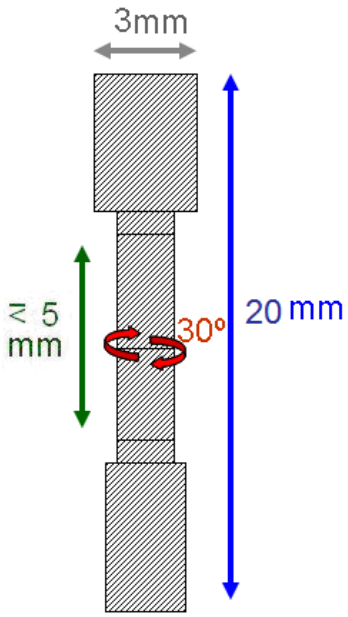

Figure 15: Design Specifications for the implant in terms of dimensions

Based on the literature review and design specifications, several alternative conceptual designs were developed. In the following sections, some of them are described in detail.

2.2 Proposed Design 1

The first idea was that the system would consist of the following parts

1. The Flexible Outer Screw
2. The Inner Screw
3. The Guide Pin
4. The Screw Driving System

In this design, the flexible outer screw is to be placed within the bones. The inner screw is to hold the flexible outer screw rigid during insertion and removed after the placement of the outer screw. The guide pin is to guide the screw system inside the bones. And, to insert the screw system in the bones, specific screw driving instruments are used. Detail explanation of these parts and how they work are explained below.

2.2.1 Outer Screw:

The main goal of the design is to create a flexible section in the middle of a bone screw which will allow the bones to have some relative movements. For demonstration purposes, it was divided into three sections, the leading edge, the flexible zone, and the trailing edge. Several ideas (Fig. 16) were generated along the course of the study to create a flexible section in the screw.

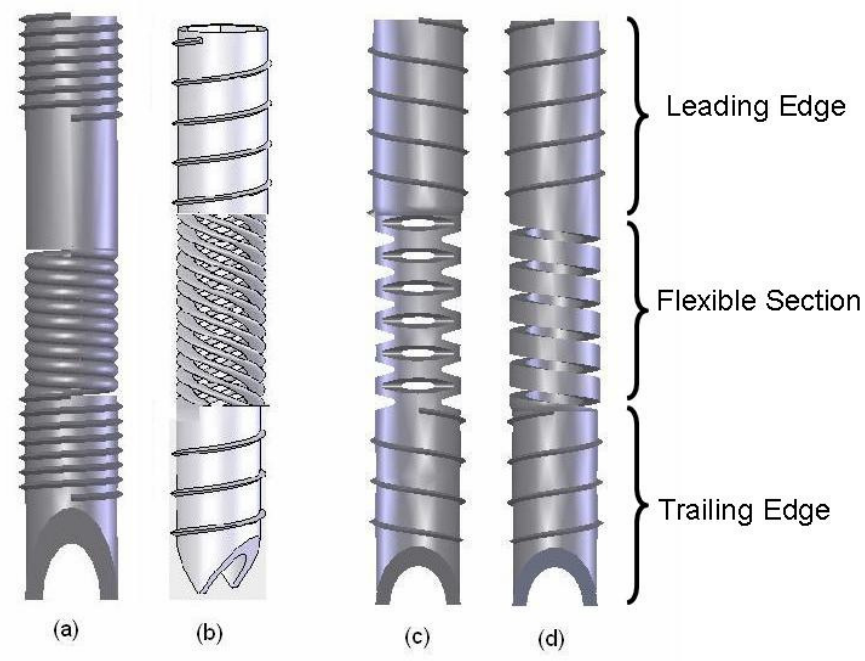

Figure 16: Different ways of creating a flexible screw (a) using spring, (b) using hollow cables, (c) by cutting notches, (d) by cutting a helical coil

The first idea involved having a spring (Fig. 16a) between the leading and the trailing edges. The advantage is that there would be no need to design and machine the flexible section. Since springs come in various shapes, forms and sizes, a specific one could be picked depending on the application. The problem arises in joining the spring to the solid section since the screw dimension is too small to weld a spring. Another potential problem is that welding changes material properties drastically which can create foreign body responses when it is used in situ. Even if it is welded successfully and was modified to overcome the foreign body response problem, independent rotation of the edges would be very difficult to achieve.

Another design involved the use of tiny helical coils (Fig. 16b) by joining one adjacent to another to create the flexible section. The advantages and disadvantages of this design technique are similar to the spring design. The mesh of tiny cables needs to be welded which is difficult and changes properties at the same time. Independent rotation of the edges may not be as difficult the spring design but still would not be possible to resolve completely.

To overcome these issues, the notch technique (Fig. 16c) was proposed. In this design, the screw can be made from a single tube without any welding or joints. Small notches will be cut from the middle in a circular pattern to obtain a flexible section. Flexibility is dependent on the angle the notches that are cut, and number of notches in one plane. The problem with this technique is that in order to make the section flexible, there

needs to be a large number of cuts with very fine machining. Other design requirements, such as independent rotation of the edges, and length of the flexible section, are difficult to fulfill. Technical drawing of this design is attached with Appendix A.

Considering the manufacturing technique for the screw, the helical coil cut design (Fig. 16d) was employed for this specific application. In this design, a helical coil area is removed from the middle section of the screw to create spring like flexibility in the middle of the screw. The advantages of this technique are, (1) it can be made from commercially available screws for this purpose, (2) cheaper compare to other designs, and (3) relatively easier to manufacture since it can be machined from a single hollow tube without any welding or joining. However, this design also does not address the independent rotation ability of the two edges. Technical drawing of one of the screws with helical coil cut is shown in Appendix B.

2.2.2 Inner Screw:

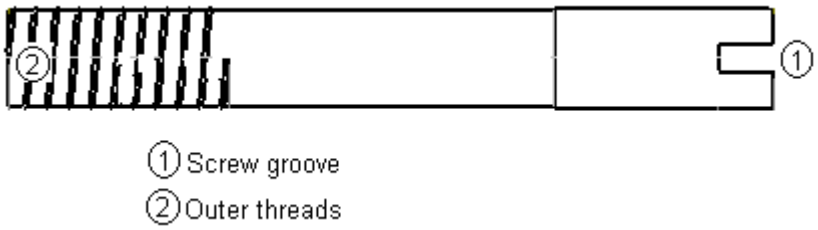

Figure 17: The inner screw, having threads only on the leading edge of the screw and a driving slot at the trailing end of the screw

The purpose of the inner screw (Fig. 17) is to keep the flexible outer screw rigid during insertion. It is a hollow cylindrical tube with threads at the tip or the leading edge and a driving slot at the end of the trailing edge. The length of the inner screw is set in a

way so that, the trailing edge of the inner screw is always below the driving slot of the outer screw. This is to prevent any interfering with the driving technique of the outer screw and thus to keep modification of the insertion instrument to a minimum.

2.2.3 Guide Pin:

The guide pin is a cylindrical solid rod. It can vary in length, and is used to guide and support both inner and outer screws during insertion of the implant into the bones during surgery. Commercial guide pins are about 1 mm in diameter. The guide pin by Zimmer® has a trochar tip which facilitates drilling into bones. The driving pin is designed to fit the screw and the driving instruments.

2.2.4 The screw driving system:

The special features of the screws and the complicated surgical procedure require a special cannulated screw driving system. This feature allows it to work around the guide pin while it tries to push the screw through the Bones. Commercially available screw driving systems has many components to them. For example, Zimmer® Herbert Whipple bone screw driving system is composed of an alignment guide, a depth gauge, a free hand guide, an insert sleeve, a free hand depth gauge, a cannulated cortical broach, a cannulated step drill, a cannulated tap, a modular handle, sleeve, screw forceps, cannulated screw driver, the OCD cannula, the OCD obturator, and cleaning tools. It also comes with a set of general instruments and optional instruments.

The focus of the study is not to redesign these instruments to fit our implant design but to design the implant in a way that these instruments can be used for its placement in bones.

2.2.5 How it Works:

During surgery, after opening the area, a dorsal incision and dorsal wrist arthrotomy is made over the SLI ligament. The scapho-lunate relationship is restored using k-wires (confirmed with direct vision and radiographic imaging). A small incision is made on the radial aspect of the wrist and under fluoroscopic (x-ray) guidance. The Guide Pin is driven across the scaphoid and into the lunate. Re-adjustments can be done if necessary to get the pin well centered in both bones on both the anteriorposterior and lateral views. A cannulated over drill creates the screw hole over the guide pin. The outer and inner screw construct is installed over the pin using a cannulated screwdriver. The inner screw maintains temporary rigidity of the construct to allow insertion. After fluoroscopic confirmation of screw placement (threaded sections of the screw is placed within each bone and the flexible section is position at the grove or in between the bones), the inner screw is removed from the outer screw using a screwdriver. Repair of the ligament or any other techniques such as capsulodesis and tenodesis can be added at the surgeon's discretion.

2.3 Proposed Design 2

In Design 1, the main focus was to create a flexible section in the mid section of the screw. The drawback of this design is that it does not permit enough relative rotation of the two edges, the leading edge and the trailing edge, to permit the motion between the scaphoid and lunate. This was addressed in Design 2 where the focus was on creating a mechanism to achieve independent rotation of the two edges. Since the edges need to rotate independently, the screw was divided into two physical parts, leading screw and the trailing screw. The design was inspired created by the simplicity of the zip-tie system. The trailing edge fits inside the leading edge and creates a connection between the bones such that the bones are able to rotate independently. There are small notches in the leading screw within which the head of the trailing screw fits and thus controls how much rotation there can be (Fig. 18). The helical cut technique is also employed to allow some bending between the bones.

The advantage of this design is that even though it has two parts, they do not require any welding or machining to join them. The design is to be manufactured as two separate parts and then snap fit together. The system is inserted into the bone as one piece during surgery. Technical drawings that were used to create a prototype of the parts are attached with appendix C1 and C2.

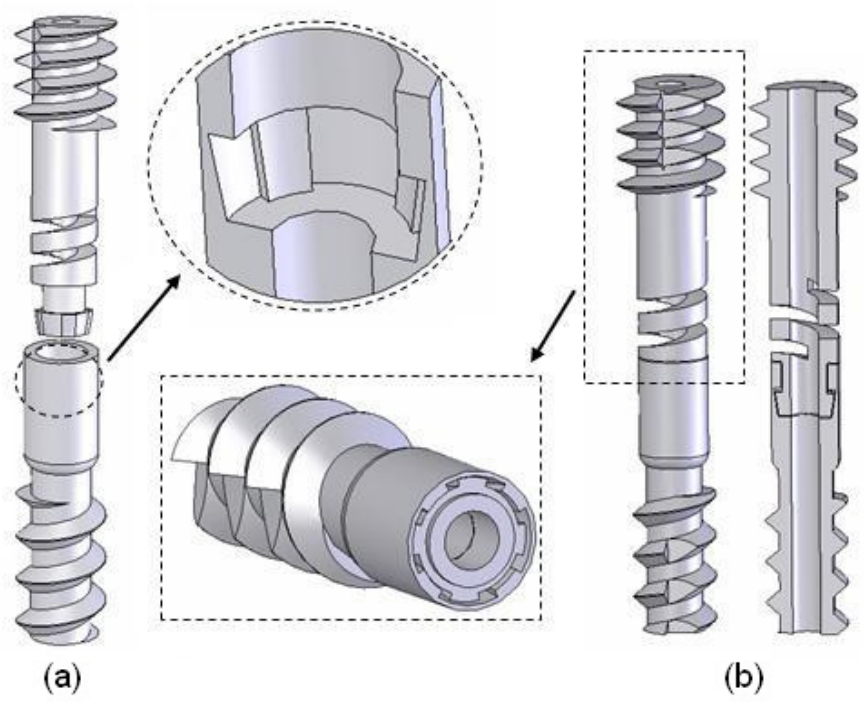

Figure 18: Zip-tie design. (a) Leading (bottom) and trailing (top) edge separately with cross section of the leading edge where the trailing edge fits. (b) Assembled screw with lengthwise cross section of the system, and vertical cross section where the two edges join.

It was found in the later stage of the study that within the given working area, having an inner screw for stabilization would be difficult and expensive to manufacture. To get around this problem, a hexagonal guide pin design is proposed as opposed to the commercially available cylindrical wire shape guide pin. The two ends of the pin are still cylindrical but the middle is hexagonal which locks itself near the leading edge. This way the guide pin still can work with commercially available insertion instruments. The cannulation of the screw is also hexagonal in the trailing edge and the mid flex section of the screw to fit the guide pin.

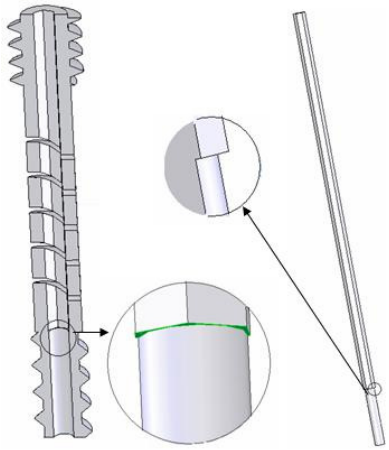

Figure 19: Hexagonal guide pin having cylindrical ends. The screw cannulation is also hexagonal except the leading edge to fit the guide pin securely.

2.4 Research issues

The goal of the study was the design and testing of a flexible bone screw which will minimize the changes in carpal kinematics after screw fixation of the SLI ligament injury. There are several issues related to the design and validation of such a screw. The main issue is the relatively small window to work with. Several techniques can be employed in the design of a flexible screw; however, carpal bones are relatively very small and designing of flexible screw implant for these bones is challenging. Testing and validating the performance of the implant in vivo should be considered to further improve the design. Manufacturing small scale implant may also need to be considered.

CHAPTER 3 FE ANALYSIS

Different materials were studied and selection was made based on the results from the analysis. The analysis was mainly performed using finite element technique. Finite Element Analysis (FEA) is a very useful analytical tool for solving mechanical design problems with complex geometry in complicated and coupled domains. It uses numerical solving techniques which are governed by the laws of physics related to the domain of the problem. FEA is cost effective, can handle complexity, and above all, it permits solving of problems without changing or simplifying the design of the problem. In this study, FEA was employed to test the strength and performance of the implant.

General steps of FEA involve classifying the problem, identifying the mathematical model, preprocessing, solving using numerical analysis, and post processing of the data. The results from FEA heavily depend on the preprocessing of parameters such as material properties, geometry, loading, boundaries, and contact conditions. When computer software is used to perform a numerical analysis, performing a preliminary analysis by solving the problem directly, if possible, is often very helpful.

Results from the FEA were used to calculate the fatigue life for the screw in different conditions. Prototypes were made for some of the designs. The notch design and the zip design were prototyped using a rapid prototyping machine and the helical coil cut was prototyped using a solid screw from Zimmer ® (Warsaw, Indiana). This chapter will

discuss different materials that were considered for the implant, method of simulation of the designs, and cadaver study.

3.1 Materials:

From organic to inorganic, there are many different types of materials that have been used as biomaterials. The materials used in orthopaedic industry comprise ceramics, polymers, metal alloys, such as stainless steel, cobalt-chromium and titanium and the shape memory alloy NiTi, bioabsorbable materials, such as bioglass, modified hydroxyapatite and bone grafts. For this study, three metal alloys, titanium, cobalt chromium, and stainless steel were used in the analysis. Material properties (Bowlin, 2006) that were used in the FEA are shown in table 1.

Ti-6Al-4V is the most common titanium alloy used in orthopedic implants because of its superior toughness, favorable mechanical properties, and excellent biocompatibility compared to other biomaterials. On average, it contains 6% Aluminum (Al) and 4% Vanadium (V) which enhances phase stabilization. However, in vivo it may release Al or V resulting in clinical failure. Furthermore, the elastic modulus of Ti-6Al-4V alloy (116 GPa) is about ten times higher than that of cortical bones (10~30 GPa), inducing the stress shielding effect between bone and implant. It is also comparatively expensive.

Cobalt chromium molybdenum's (Co-Cr-Mo) primary advantage is its corrosion resistance in chloride environments. However, its elastic modulus is about two times higher than the Ti-alloy. It also releases metallic ions like Ti alloy, resulting in clinical failure.

Among many different stainless steel alloys, SS 316L is primarily used for implants because of its superior biocompatibility and corrosion resistance. It is also inexpensive compared to the other two alloys. The elastic modulus of SS 316L is not as high as Co-Cr-Mo, but still is higher than Ti alloy (about 1.6 times) as well as the bone.

In this study, the usability of the materials was tested by comparing the resulting maximum von Mises stress on the implant. Their biocompatibility and corrosion resistance comparison were beyond the scope of this study.

Table 1: Material properties of the metal alloys used in the FEA

Materials	Elastic Modulus (GPa)	Tensile Strength (MPa)	Poisson's Ratio
Ti-6Al-4V	116	965	0.3
Co-Cr-Mo	210	655	0.3
SS 316L	190	586	0.3

Two other types of materials, plastic and bioabsorbable polymer, may have some potential for this implant. However, testing the materials for this implant was beyond the scope of this study. Some of their pros and cons are explained here.

Use of plastic materials are promising for the flexible screw from the flexibility and manufacturing point of view. However, their mechanical properties change very quickly over time as it goes through cyclic loading, when compared to metallic alloys. Bioabsorbable polymers, as the name implies, are absorbed by the body. The advantage of using this material as for the implant is that the patient does not need to go for a removal surgery of the implant. It also has the disadvantage in terms of response in the body.

The use of bioabsorbable polymers is becoming increasingly popular in orthopaedics (Spitalny, 2006). However their use is still controversial in literature. In a study, Short, Werner, and Sutton supported the use of a bioabsorbable polymer plate for the treatment of scapholunate injury with the recognition that the material may causes a foreign body reaction in-vivo. They tested the plate under cyclic loading on cadaver wrists. For the materials, they used Polylactic acid (PLA) for the plate material and nylon for the screws that connect the plate with the bone. The PLA materials degrade in a period of two to four years (Short, Werner, and Sutton, 2008). Figure 20 shows the plate used in their study on cadaver wrist.

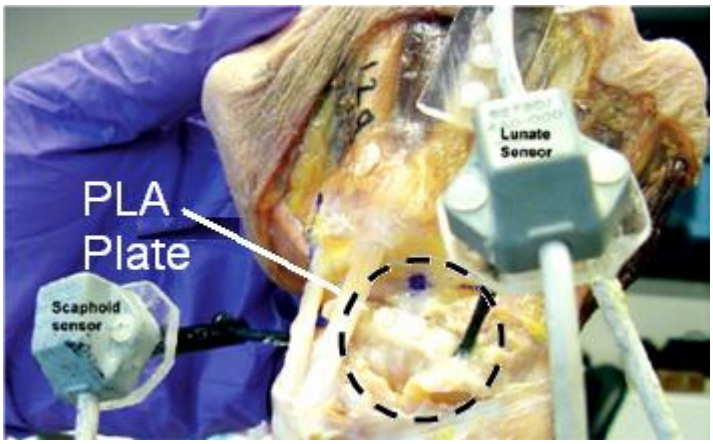

Figure 20: Bioabsorbable polymer plate tested in cadaver to join scaphoid and lunate. The circled area shows the PLA (Polylactic acid) plate in white (Image modified from Short, Werner, and Sutton, 2008)

One of the problems with bioabsorbable materials is that their responses are difficult to determine since the response may be patient dependent. This implies that, one material may be well tolerated in one patient and the same material may cause serious inflammatory reaction in another. Two of the most common biomaterials used for upper

arms are polylactic acid or ploylglycolic acid. As these materials degrade with time, they create very acidic local environment which leads to bone absorption of the bone. In any situation this type of inflammatory response would be catrostrophic. Thus only metallic materials were considered in the design of this study.

3.2 FE Analysis Conditions:

SolidWorks (Dassault Systèmes SolidWorks Corp, ©2008) was used for modeling the geometry and performing FEA on the geometry as a method of testing the designs. The software package offers integrated solid modeling and FEA. It is well known for design, analysis, and product data management in this field. The most useful feature of this software is that it enables generating a very complex solid model. And without any conversion or transfer mid step, it is possible to perform a stress analysis on the created solid body.

The first step of preprocessing for FEA is creating the geometry. Three dimensional models of the designs were created in SolidWorks platform. It also helped in getting a better understanding of the design, creating rapid prototype, and machining. From a manufacturing point of view, the notch design and the helical coil cut design have many advantages, and therefore were modeled for analysis. From concept Design 2, the leading and trailing edge assembly with a helical cut in the trailing edge was created for analysis.

Boundary conditions were applied to these geometries based on the understanding of the kinematics and biomechanics of the wrist. It was described in section three of Chapter one that the wrist supports a significant amount of load in daily activities. If it is

assumed that the weight at the tip of the finger is about 10 lb or about 5 Kg, then, based on the study by Garcia-Elias, the applied force on the carpal bone can be assumed to be about 50 N, distributed on all of the eight bones (Garcia-Elias, 1996). However, the magnitudes of the distributed force on individual carpal bones are unknown. Furthermore, the biggest problem is that, 50N may not be the maximum load that the carpal bones will be exposed to in all situations. In order to get around this problem, studies were performed using displacements in place of loads. Using the solid model, the following set of analysis was performed:

Case 1: Bending to analyze different planner movement

Case 2: Compression and tension to analyze results of capitate head push

Case 3: Individual relative rotation between the edges

Case 1: The motivation for case 1 was to analyze different wrist motions (Fig. 5).The screw was bent from one end while the other end was fixed. A free body diagram of this case is shown in figure 21a. 1 to 5 mm of displacement was applied with a 0.25mm increment to bend the screw to calculate flexibility of the system.

Case 2: the motivation for case 2 was to analyze the potential movement of the bones with adjacent bones causing them to compress or expand. This was done by fixing one end of the screw and by applying displacement to the other end of the screw to cause it to undergo tension or compression. The simplified free body diagram is shown in figure 21b. In this configuration, 0.1 to 1mm of displacement was applied with 0.1mm increment.

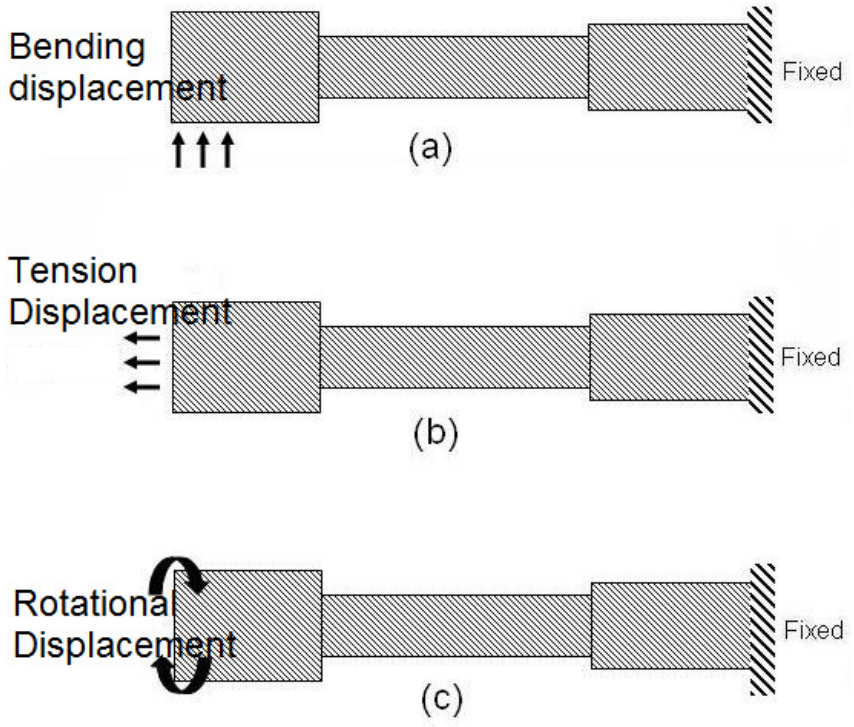

Figure 21: Boundary conditions applied during FEA. (a) Bending in case 1, (b) tension in case 2, and (c) rotation in case 3

Case 3: The motivation for case 3 was to analyze the relative motion between the bones by applying rotational displacement to the ends of the screw keeping the other end fixed. Figure 21c is a free body diagram showing the displacement and boundary. In this configuration, 0.1 to 1 radian (~ 6º to 60º) displacement was applied with 0.1 radian increment to find maximum rotation that is possible by the system.

Both combinations, leading edge fixed and tailing edge displaced, and leading edge displayed and tailing edge fixed, were done for all of these cases.

Following creating of the solid model, a finite element mesh consisting of tetrahedral element was generated on the notch, helical coil, and zip-tie designs (Fig. 22).

Since the size of the smallest feature is 0.05 mm in every design, a convergence test was not performed for every single design but only for the helical coil cut design. First the mesh was applied based on the smallest feature; 0.05 mm global size with tolerance 0.0025 mm. For this size mesh, the number of elements and nodes generated were beyond the capability of the computer used. Therefore, a convergence test was done and found that a mesh size of 0.4 mm global size produced a converging result. This mesh size gave a total of about 20856 nodes and 11438 elements for the 22 mm helical coil cut design. A snapshot of the mesh is shown in figure 22. This mesh size, however, was not applied to the notch design. For the notch design a mesh size of 0.2 mm global size was applied for its small features.

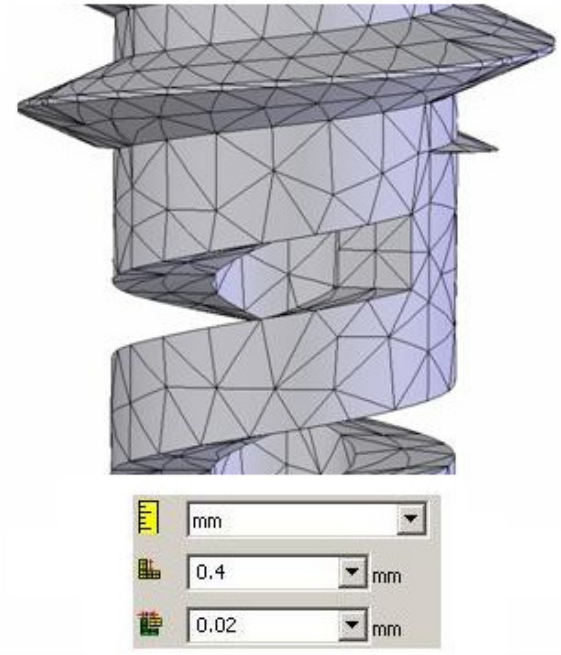

Figure 22: Example of mesh applied to a screw with global size of 0.4 mm and tolerance of 0.02 mm

3.3 FE Analysis Results:

Analysis was performed on the following seven designs:

(1) 22 mm long screws with helical coil cut

(2) 24 mm long screws with helical coil cut

(3) 26 mm long screws with helical coil cut

(4) Helical coil cut screw with optimized flexibility

(5) The zip-tie screw

(6) The notched screw

(7) Solid Zimmer screw

Three materials were tested:

(1) SS 316L

(2) Co-Cr-Mo

(3) Ti-6Al-4V

The simulations were performed in three different displacement conditions:

(1) Bending

(2) Tension

(3) Torsion

First materials were tested using the helical coil cut screw. Then individual screws were studied using the results from the material test. In all cases, the maximum vonMises stress, and the resulting force or moment was calculated and plotted over applied displacement. A preliminary analysis was done to compare the results from the

simulations. A fatigue analysis was performed in order to calculate the number of cycles to failure for the screw.

3.3.1. Material Test Results

Testing every material in every design would lead to a large number of analyses. Hence, it was assumed that if one material worked better for one particular design, it should do the same for all the others. Therefore all three materials were tested on the helical coil cut screw to find the best material fit for the implant. The helical coil cut design was used with the 22 mm, 24 mm, and 26 mm long screws. Here, it needs to be mentioned that the available prototype led to chose this length, not the design criteria. A comparison of the results is shown in Figure 23. It was found that the resulting stress on Titanium was less than other materials. Therefore, Titanium was used as the material for the rest of the study. Along with the best performance in stress analysis, there were more reasons for selecting Titanium. The most important one is that most rigid screws that are out in the market presently are also made out of Titanium. Therefore, comparing the proposed designs with the current products using Titanium material properties was reasonable.

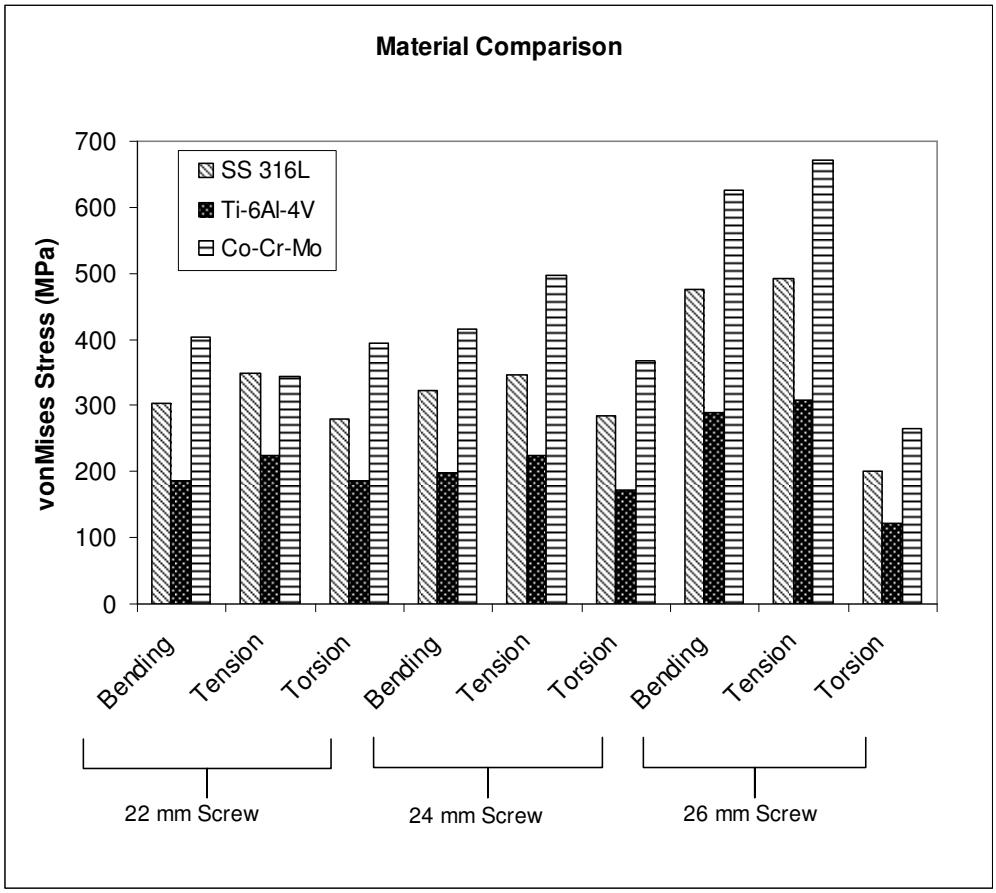

Figure 23: FEA result of Material Comparison test. 0.1 mm tension, 1mm bending and 0.1 radian torsion was applied to 22 mm, 24 mm, and 26 mm length screws with the helical coil cut design and in every case, three materials properties were applied consecutively, SS 316L, Ti-6Al-4V, and Co-Cr-Mo. The darker column shows stress resulted from Titanium and is less than the other two materials, stainless steel and Cobalt Chromium

3.3.2 Preliminary Analysis:

A preliminary analysis was performed to calculate the reaction force and stress for a given displacement. In order to perform the analysis, a solid block was created in FEA with 1 x 1 x 1 mm dimensions. Therefore it has 1 element and 2 nodes. Displacement was applied to node 2 while node 1 was fixed. Resulting stresses were calculated using the

simplified axial displacement approach. Figure 24 is a free body diagram of the simplified problem analysis and the following equations were used for the calculation.

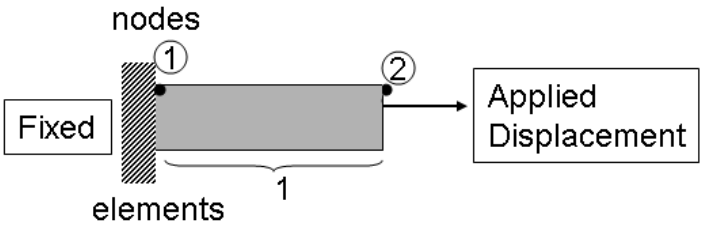

Figure 24: Free body diagram used in the preliminary calculations with a single block of 1x1x1 m dimension. Displacement was applied to node 2 while node 1 was fixed.

$$\underline{f} = [\mathrm{k}]\ \underline{u} \qquad \text{.....(1)}$$

$$[\mathrm{k}] = \frac{EA}{L}\begin{bmatrix} 1 & -1 \\ -1 & 1 \end{bmatrix} \qquad \text{.....(2)}$$

$$\overline{\sigma} = \frac{f}{A} \qquad \text{.....(3)}$$

Force was calculated for the given displacement using equation (1) and (2). Using the resulting force (N), stress (MPa) was calculated on the area. Using this equations, reaction force was calculated to be 1.08e8 N and stress was 1.08e2 MPa. Similar results were obtained from FEA. The resulting reaction force on the block was 1.0829e8 N, 1st principle stress was 2.38e2 MPa, and von Mises stress was 2.88e2 MPa. Figure 25 shows a screen shot of the FEA using SolidWorks. The force result obtained from FEA and preliminary analysis matches with each other. However the stress analysis results do not match. In preliminary analysis, the area before deformation was used as the cross sectional

area. However, in computer simulation, it may take the cross sectional area after deformation and hence stress is larger.

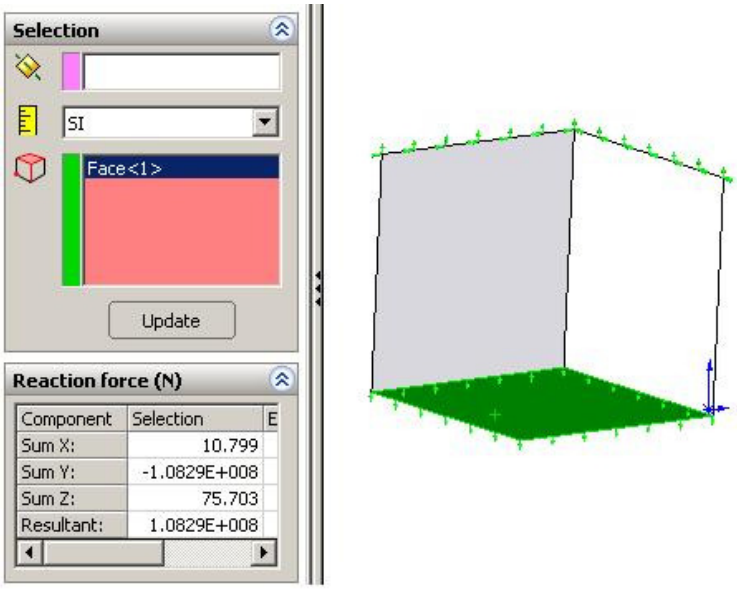

Figure 25: Sample FEA calculation to compare the FEA calculations with the preliminary analysis. 1x1x1 m block was fixed on the top surface and the displacement was applied to the bottom surface. Reaction force at the bottom surface was calculated to be 1.0829E8 N.

3.3.3 FE Analysis to determine Maximum von Mises Stress and Reaction Force:

After the material selection, all seven designs were analyzed using Titanium material properties under different loading conditions. From every simulation, maximum von Mises stress and Reaction Force at the area of applied displacement were calculated. The von Mises stress, also known as the maximum distortion energy criterion, determines the failure criteria of the material when the energy of distortion reaches the same energy for yield or failure in uniaxial loading conditions. Although yielding is caused by shear stress, the maximum shear stress occurs on three planes. This is why the von Mises stress

has a greater chance on a statistical basis of finding the failure of the material. The reaction force was calculated in order to determine how much force it required for the screw to bend or rotate for a given displacement.

The first set of simulations was conducted on three different helical coil cut designs. The design was then optimized for maximum flexibility based on the design criteria. The third set of simulations was done on the zip-tie design. Finally, the optimized helical coil cut, the zip-tie, and notch designs were compared with a solid screw model. All of these simulations were conducted by applying bending, tension and torsion conditions.

3.3.3.1 Helical Coil Cut Design Simulation:

The helical coil cut technique was applied in three different length screws. For all the screws, a different flexibility was designed as given by the prototyping company (Fig. 26). For all three screws, the flexure length was fixed to 7.14 mm. The variations are shown in Table 2. Three sets of simulations were performed by applying (1) 1-5 mm of bending with 0.1 mm increment, (2) 0.1-1 mm of tension with 0.01 mm increment, (3) and 0.1-1 radian of torsion again with 0.01 mm increment, condition. In every case, incremental simulation was stopped when the resulting stress on the screw was larger than the yield stress of the material. The reaction force at the area of applied displacement was also calculated. The results are shown in Figure 27 – 37 with their contour plots. The tabulated results are shown in Table 3.

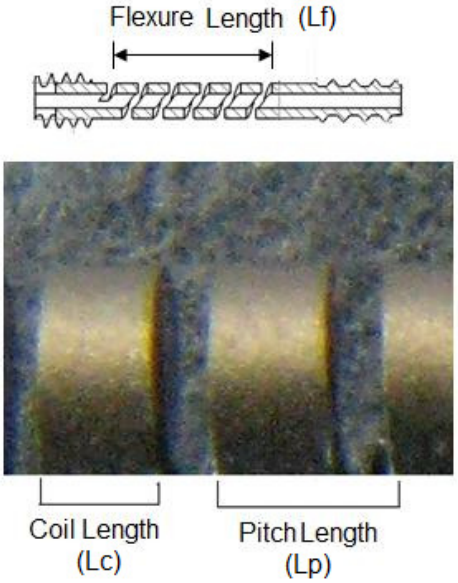

Figure 26: Flexure, coil and pitch length on the helical coil cut screw. The top image shows the flexure length and the bottom image shows coil length and pitch length under microscope which was applied in the solid model

Table 2: Pitch and coil length used for helical coil cut design as done by the prototyping company

Screw Length (mm)	22	24	26
Pitch Length (mm)	1.4	1.5	2.2
Coil Length (mm)	0.85	0.9	1.5

The purpose of the simulation was to determine which one of these screws was more flexible. In comparison of these screws, it was found that the 22 mm long screw was more flexible than the other two screws. It was 24.7% more flexible than the 24 mm long screw and 33.4% more flexible than the 26 mm long screw.

Table 3: Helical coil cut design simulation result

22 mm								
Bending			Tension			Torsion		
disp(mm)	Stress(MPa)	Force (N)	disp(mm)	Stress(MPa)	Force (N)	disp(rad)	Stress(MPa)	Moment (N-mm)
4.1	764.78	2.23	0.32	705.93	26.09	0.51	849.4	6.08
4.2	783.43	2.28	0.33	728	26.9	0.52	866.05	6.19
4.3	802.09	2.34	0.34	750.06	27.72	0.53	882.71	6.31
4.4	820.74	2.39	0.35	772.11	28.53	0.54	899.36	6.43
4.5	839.39	2.44	0.36	794.17	29.35	0.55	916.02	6.55
4.6	858.05	2.5	0.37	816.24	30.16			
4.7	876.7	2.55	0.38	838.31	30.98			
4.8	902.07	2.61	0.39	860.37	31.79			
4.9	922.16	2.66	0.4	882.43	32.61			
5	932.66	2.72	0.41	904.49	33.43			

24 mm								
Bending			Tension			Torsion		
disp(mm)	Stress(MPa)	Force (N)	disp(mm)	Stress(MPa)	Force (N)	disp(rad)	Stress(MPa)	Moment (N-mm)
3.1	738.03	2.19	0.31	848.17	33.46	0.41	823.19	9.16
3.2	761.83	2.26	0.32	875.53	34.54	0.42	843.27	9.37
3.3	785.64	2.33	0.33	902.89	35.62	0.43	863.34	9.52
3.4	809.45	2.41				0.44	883.42	9.74
3.5	833.26	2.48				0.45	903.5	9.97
3.6	857.06	2.54						
3.7	880.07	2.62						
3.8	904.68	2.69						
3.9	928.48	2.76						
4	952.29	2.84						

26 mm								
Bending			Tension			Torsion		
disp(mm)	Stress(MPa)	Force (N)	disp(mm)	Stress(MPa)	Force (N)	disp(rad)	Stress(MPa)	Moment (N-mm)
2.5	725.057	3.19	0.21	646.28	49.09	0.41	869.36	20.58
2.6	754.06	3.32	0.22	677.05	51.43	0.42	890.49	21.08
2.7	783.06	3.44	0.23	707.82	53.77	0.43	912.06	21.59
2.8	812.06	3.58	0.24	738.61	56.11			
2.9	841.06	3.72	0.25	769.38	58.45			
3	870.06	3.83	0.26	800.15	60.79			
3.1	899.06	3.97	0.27	830.9	63.12			
			0.28	861.69	65.46			
			0.29	892.47	67.8			
			0.3	923.25	70.14			

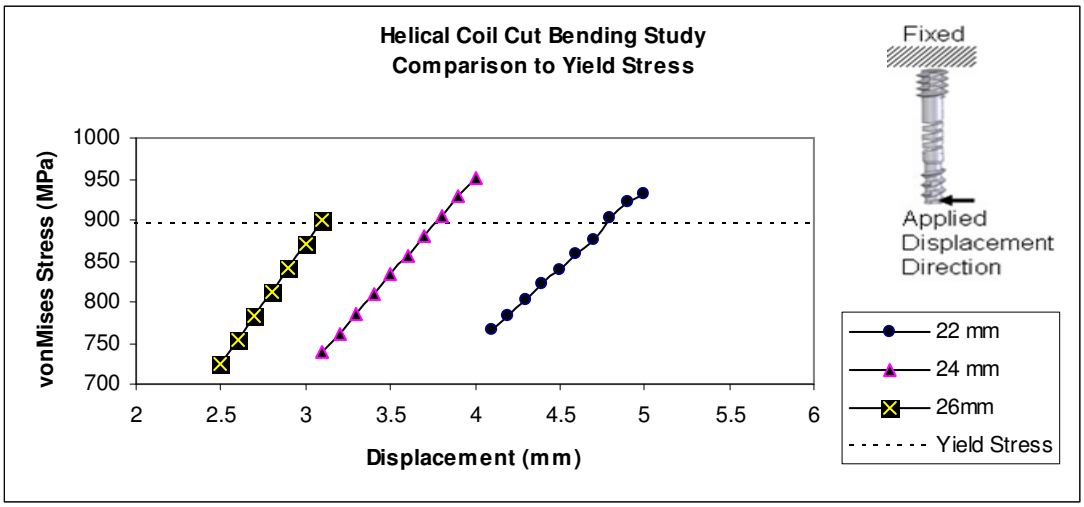

Figure 27: Maximum vonMises stress distribution of the bending study of the helical coil cut design. The result indicates that the 22 mm screw can bend the most (4.7 mm) before deforming permanently. The 24 mm screw can bend up to 3.7 mm and the 26 mm screw can bend up to 3 mm before deforming permanently

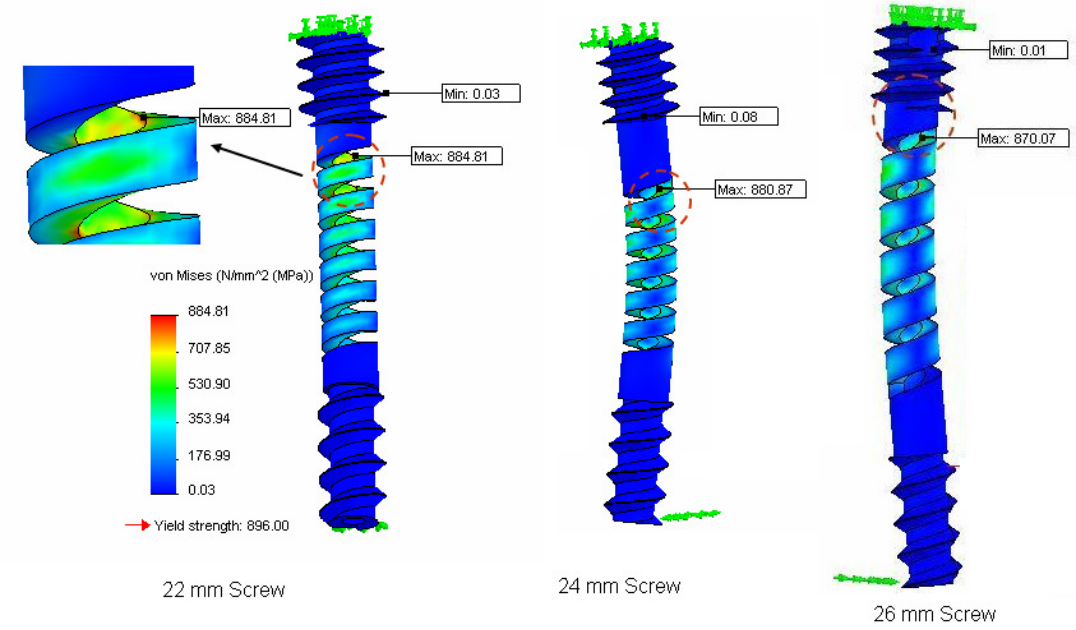

Figure 28: Contour plot showing maximum vonMises stress distribution of bending before permanent deformation of the helical coil cut screw, maximum stress occurs at the flexible section in opposite side from the applied displacement area. The deformation is about 4 times larger than true scale

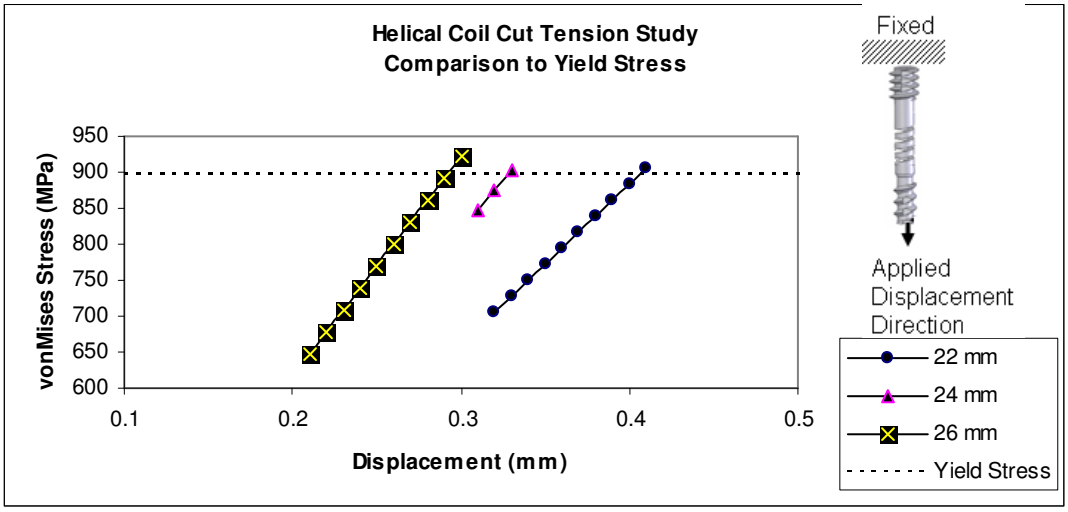

Figure 29: Maximum vonMises stress distribution of the Tension study of the helical coil cut design. The result indicates that the 22 mm screw can elongate the most (0.4 mm) before deforming permanently. The 24 mm screw can elongate up to 0.32 mm and the 26 mm screw can elongate up to 0.29 mm before deforming permanently.

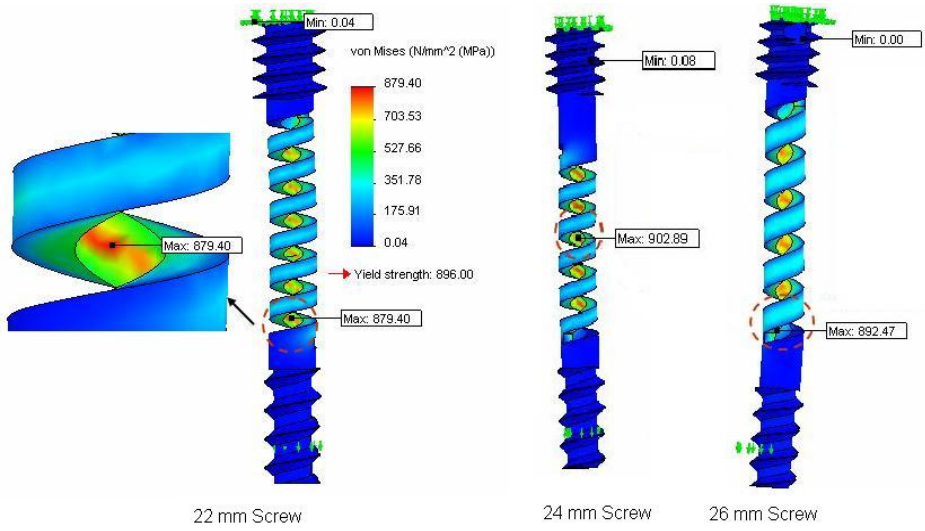

Figure 30: Contour plot showing vonMises distribution in elongation before permanent deformation of the helical coil cut screw, maximum stress occurs at the flexible section in all cases, for the 22 mm screw it is near the leading edge, for the 24 mm screw it is at the middle, and for the 26 mm screw it is again near the leading edge of the flexible area of the screw. The deformation is about 4 times larger than true scale

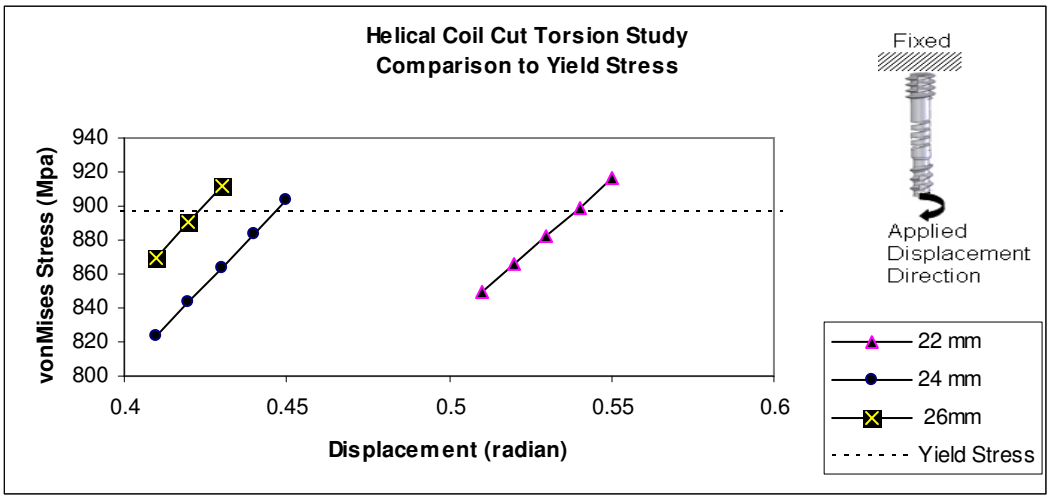

Figure 31: Maximum vonMises stress distribution of the torsion study of the helical coil cut design. The result indicates that the 22 mm screw can rotate the most (up to 0.54 radian or 30º) before deforming permanently. The 24 mm screw can rotate up to 0.44 radian or 25º and the 26 mm screw can rotate up to 0.42 radian or 24º before deforming permanently

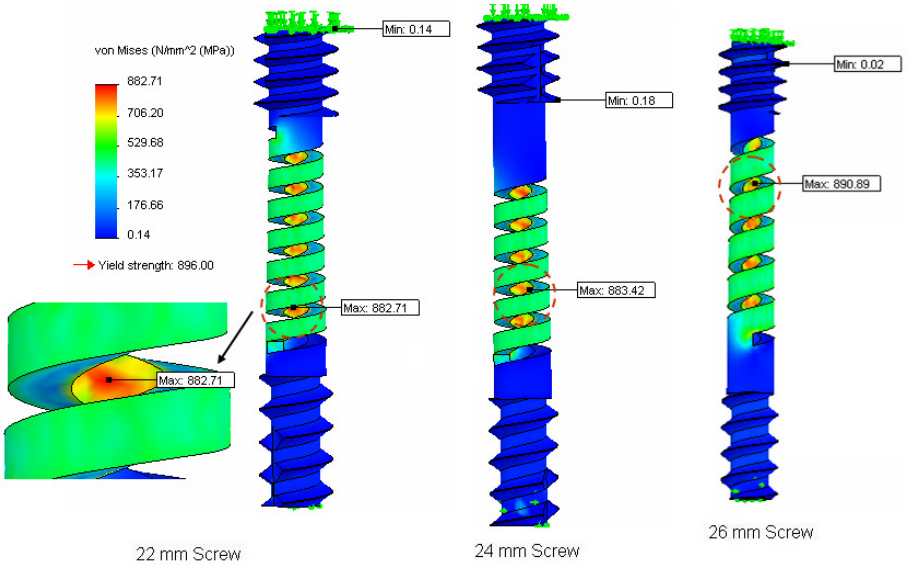

Figure 32: Contour plot showing maximum von Mises stress results of torsion study before permanent deformation of the helical coil cut screw. Maximum stress occurs at the flexible section in all cases, for the 22 mm screw it is near the leading edge, for the 24 mm screw it is near the middle, and for the 26 mm screw it is near the trailing edge flexible area of the screw. The deformation is not a true scale deformation.

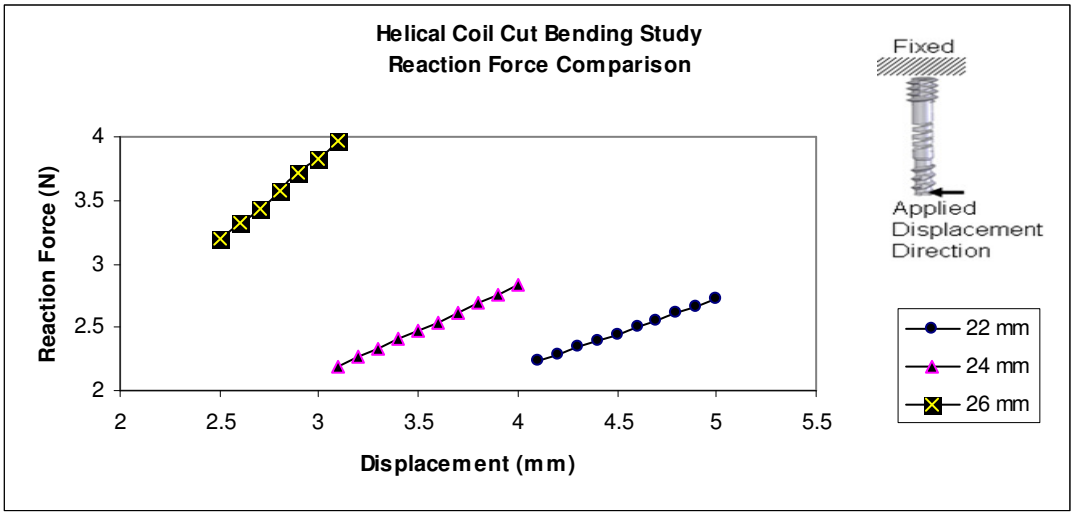

Figure 33: Reaction force in the area where displacement was applied, for all 22, 24, and 26 mm screws as a result of bending. The graph shows that it required less force to bend the 22 mm screw than the 24 or 26mm screw. The maximum force was required for the 26 mm screw and the 24 mm screw fell in the middle

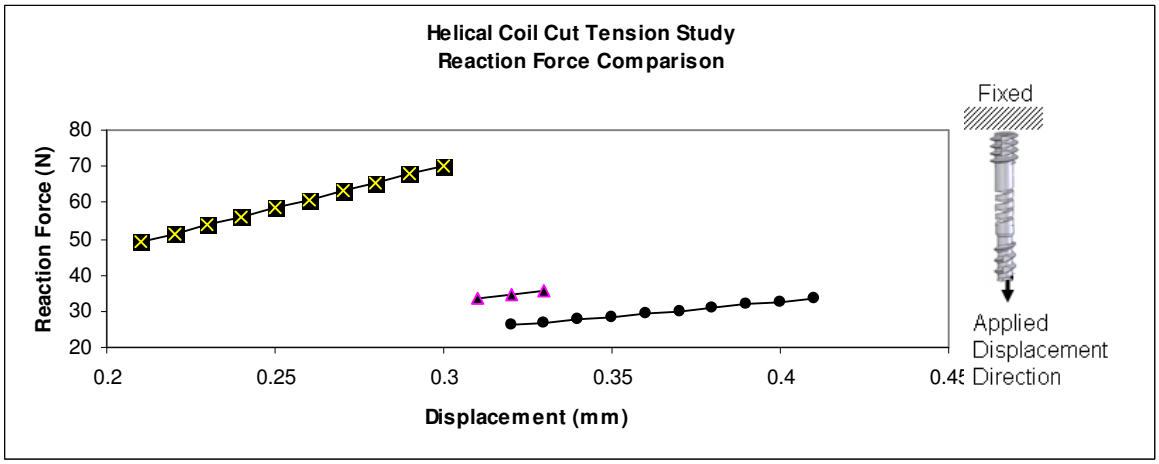

Figure 34: Reaction force in the area where displacement was applied, for all 22, 24, and 26 mm screws as a result of tension. The graph shows that it requires less force to elongate the 22 mm screw than the 24 or 26mm screw. The maximum force was required for the 26 mm screw and the 24 mm screw fell in the middle

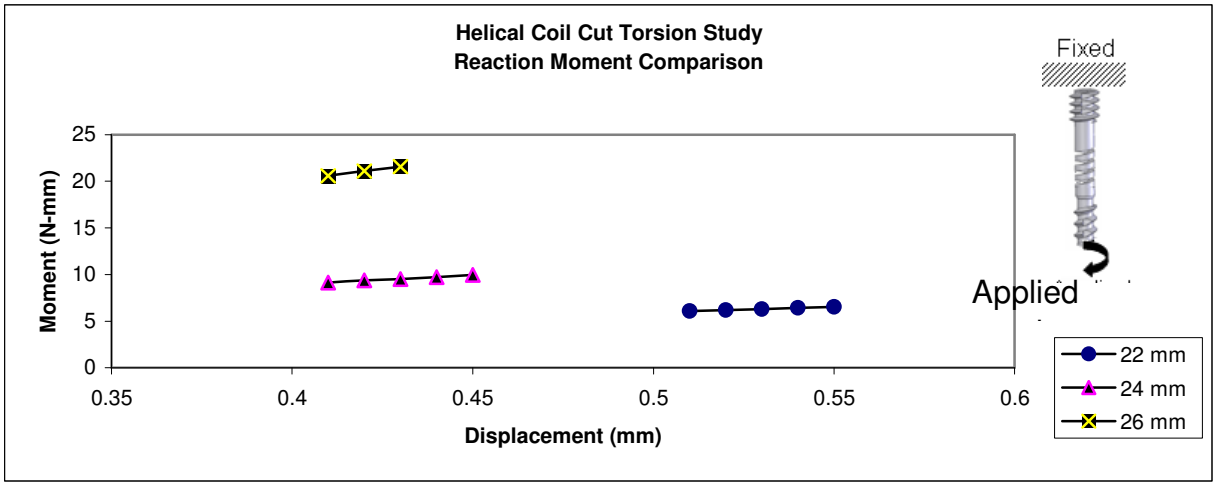

Figure 35: Reaction moment in the area where displacement was applied, for all 22, 24, and 26 mm screws as a result of torsion. The graph shows that it requires less force to rotate the 22 mm screw than the 24 or 26mm screw. The maximum force was required for the 26 mm screw and the 24 mm screw fell in the middle. All screws have the same dimension at the trailing edge and leading edge sections where displacement was applied

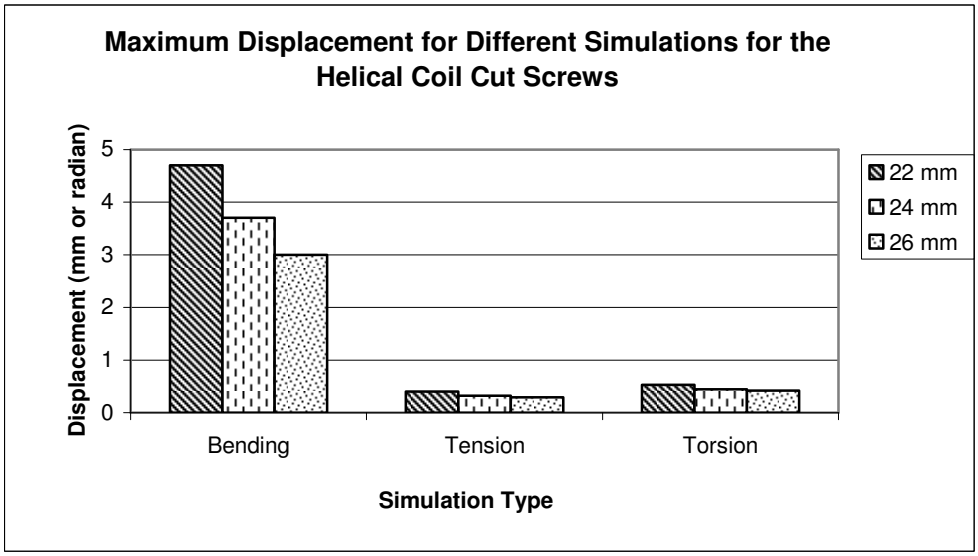

Figure 36: Combined result of the simulations performed on the three different length helical coil cut screws in three different displacement conditions showing maximum displacement. The screw performs the best in bending condition and the 22 mm long screw performs the best in all cases than the 24 mm and 26 mm long screws

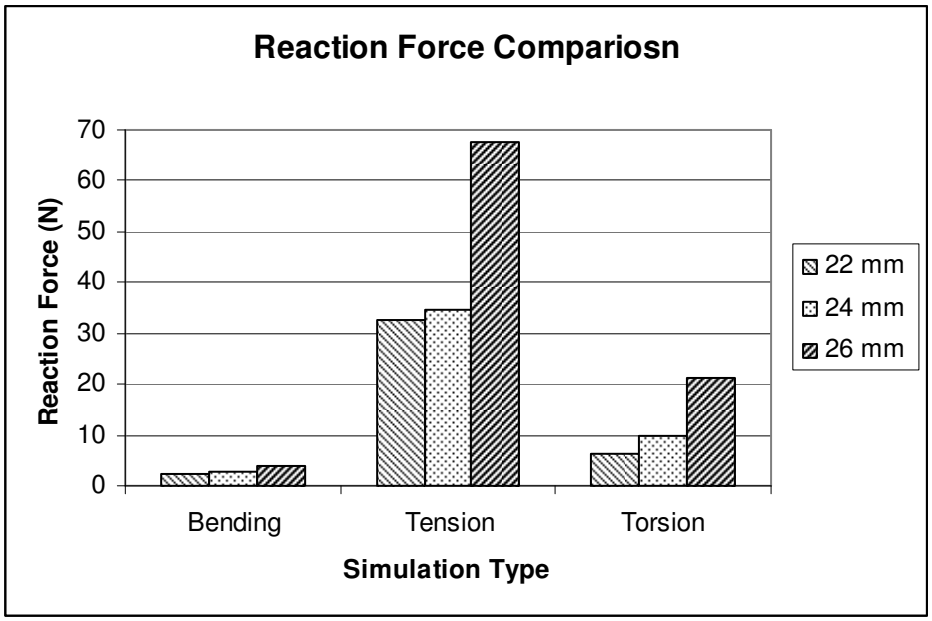

Figure 37: Combined result of the simulations performed on the three different length helical coil cut screws in three different displacement conditions showing the reaction force. The screw performs the best in bending condition and the 22 mm long screw performs the best in all cases than the 24 mm and 26 mm long screws

3.3.3.2 Optimization Simulation

Following the stress study, an optimization study was performed to find the optimum coil length (L_c) and pitch length (L_p) ratio for the helical cut (Fig 38). For this optimization study, the screw length was 22 mm since the smaller the screw, the better it is for its function. The coil length was varied from 0.3 – 1.0mm, because smaller dimentions are very difficult to manufacture. The spring length was fixed to be 5mm since one of the design criteria for the flexible section is that it can not be greater than 5 mm. Titanium material properties were used for all because it showed the best results in previous study. The different ratios of (L_c/L_p) were applied to the design, 1:2, 1: 2.5 and 1: 3. The

simulations were performed applying 5 mm of bending at the trailing edge while keeping the leading edge fixed.

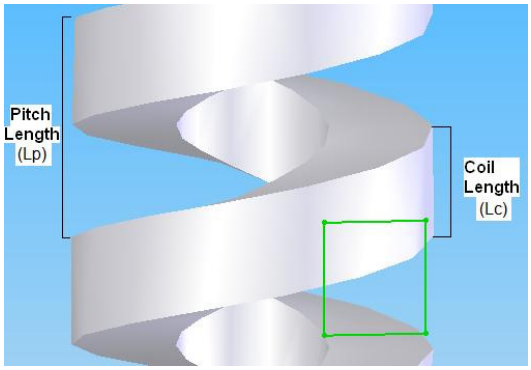

Figure 38: Flexible cut was simulated to find the optimized coil and pitch length ratio.

Table 4: Optimization Study Results

$(L_c)/(L_p)$	Pitch Length (mm)	Revolution	Coil Legnth (mm)	Maximum von Mises Stress (Mpa)	Force (N)
$(L_c)/(L_p)$ = 1:2	0.60	8.33	0.30	365.00	2.28
	0.70	7.14	0.35	461.04	2.41
	0.80	6.25	0.40	604.75	2.80
	0.90	5.56	0.45	784.00	3.11
	1.00	5.00	0.50	881.48	3.33
$(L_c)/(L_p)$ =1:2.5	0.75	6.67	0.30	403.34	2.81
	0.88	5.71	0.35	470.57	2.90
	1.00	5.00	0.40	637.79	2.98
	1.13	4.44	0.45	805.02	3.13
	1.25	4.00	0.50	922.24	3.35
$(L_c)/(L_p)$ = 1:3	0.90	5.56	0.30	823.00	3.73
	1.05	4.76	0.35	960.17	3.89
	1.20	4.17	0.40	1097.33	4.04
	1.35	3.70	0.45	1234.50	4.20
	1.50	3.33	0.50	1371.67	4.39

The result showed that for the given conditions, the coil and pitch length ratio of one to two (1:2) featured in the minimum stress and reaction force. The results are

presented in Table 4 and Figure 39. The shaded area on the table shows the optimized ratio of pitch and coil length. When this ratio is one to two (1:2) which mean the pitch length is double of the coil length, stress is minimum on the flexible section for a given displacement. The reaction force is also relatively smaller for this ratio.

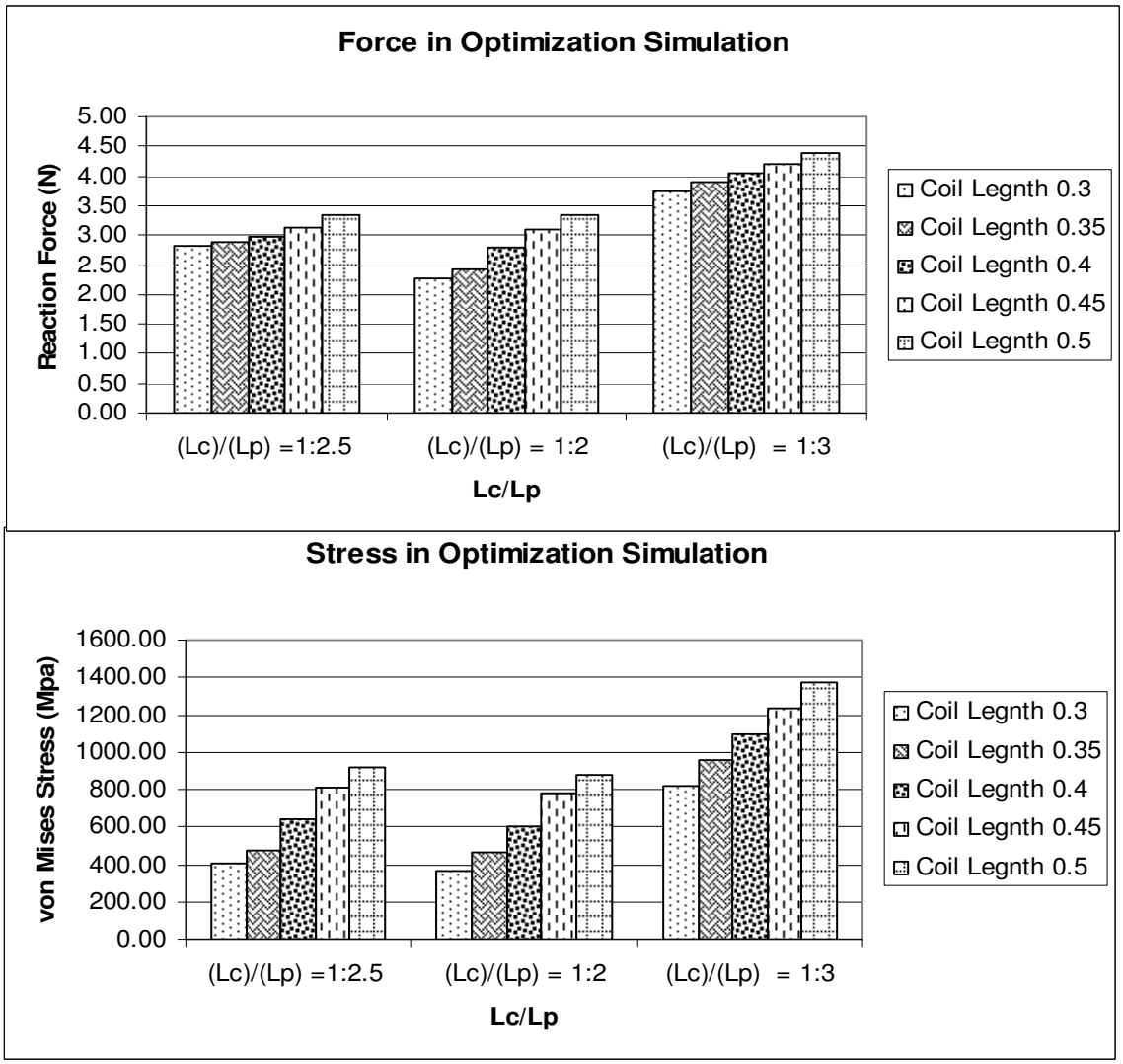

Figure 39: Optimization analysis results displaying the maximum von Mises stress and reaction force at the applied displacement area. The top graph plots the maximum von Mises stress and the bottom graph plots the reaction force over $(L_c)/(L_p)$ ratio. The middle darker column presents the result of the study when the $(L_c)/(L_p)$ was one to two (1:2) and performed better than other two ratios applied.

3.3.3.3 Zip-tie Design Simulation

Three different types of simulations were performed on the zip-tie screw as well, 1-5 mm of bending, 0.1-1 mm of tension, and 0.1-1 radian of torsion. The length of this screw was 10 mm. The screw system was able to bend up to 2.7 mm, elongate up to 0.16 mm and rotate up to 36º before deforming permanently, the resulting reaction forces at the surface where deformation was applied were 1.24 N at bending, 14.7 N tension and the reaction moment was 63.47 N-mm at torsion. The contour plots are shown in Figures 40-42 for different loading conditions.

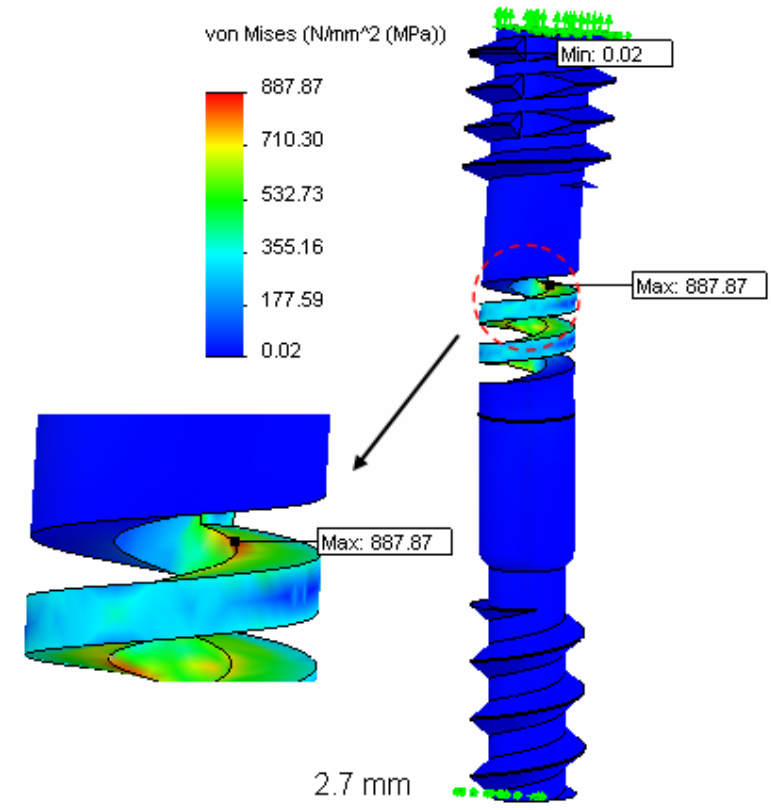

Figure 40: Resulting stress from bending on the zip-tie design. The screw system was able to bend up to 2.7 mm before deforming permanently, reaction force at the surface was found to be 1.24 N where bending was applied

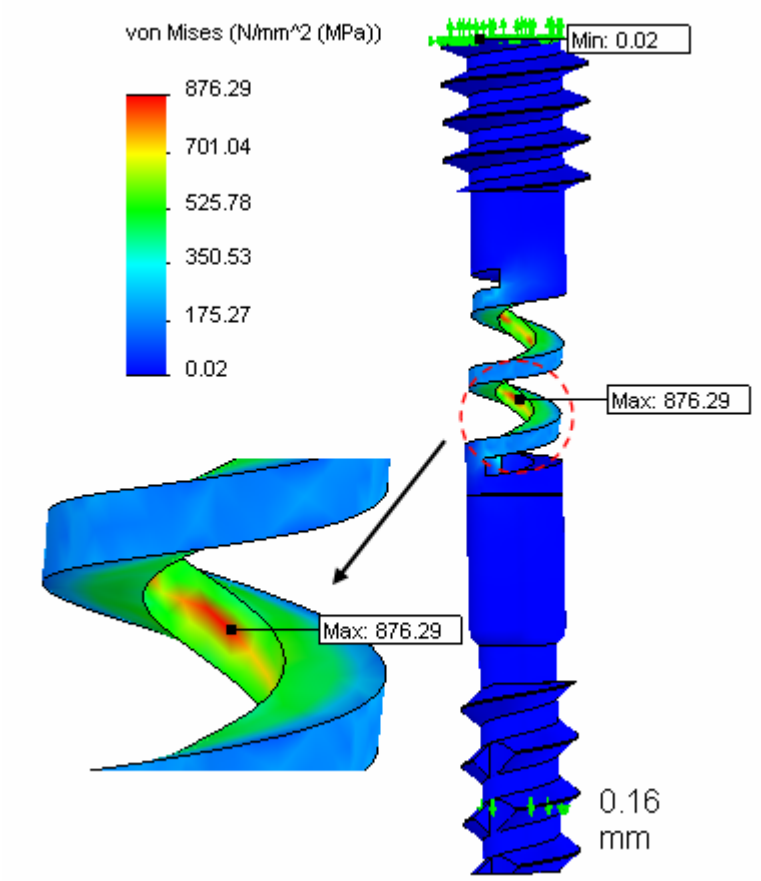

Figure 41: Resulting stress from tension on the zip-tie design. The screw system was able to elongate up to 0.16 mm before deforming permanently, reaction force at the surface was found to be 14.7 N where tension was applied

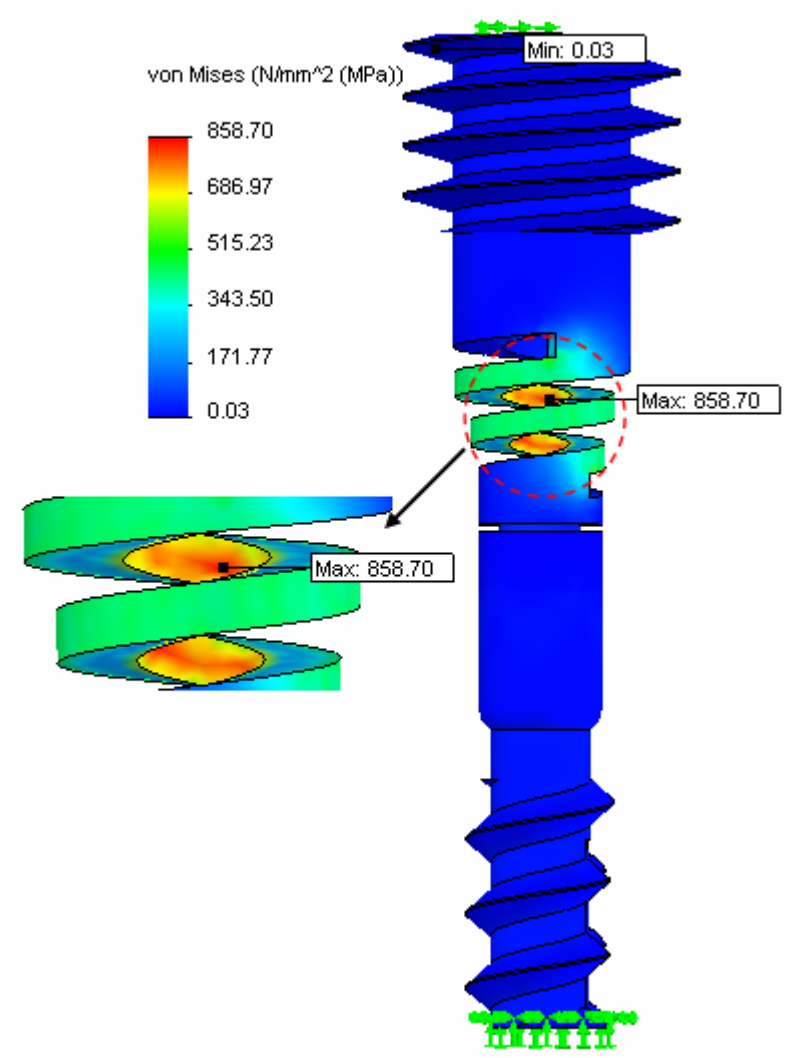

Figure 42: Resulting stress from torsion on the zip-tie design. The screw system was able to rotate up to 36º before deforming permanently. Total reaction moment was found to be 63.47 N-mm at the surface where rotation was applied

3.3.3.4 Comparison of Different Screw Designs:

For the comparison analysis, a solid 22 mm long screw was modeled. The solid screw replicates one of the commercially available screws from Zimmer® (Warsaw, Indiana). Four different models were compared, (1) the solid screw from Zimmer®, (2) the notch design, (3) the optimized helical coil cut design, and (4) the zip-tie design. They were all tested in three different loading conditions: 2.5 mm bending, 0.3 mm tension, and 30º torsion. The results are summarized in Table 7 and plotted in Figures 43-48 with contour plots.

In all cases, the zip-tie and helical, both show much smaller stress than the solid or notched screw. In bending the helical coil cut performs better than the zip-tie design. And in torsion the zip-tie performs better than the helical coil cut design. The notch design shows maximum stress of all and the solid screw had the maximum reaction force.

Table 5: Reaction force and maximum von Mises stress in comparison Study

Solid Design		Notch Design		Optimized Helical Coil Cut Design		Zip-tie Design	
Stress (MPa)	Reaction Force (N)	Stress (MPa)	Reaction Force (N)	Stress (MPa)	Reaction Force (N)	Stress (MPa)	Reaction Force (N)
Bending							
3247	148.62	2.67e4	639.90	440.74	0.66	814.52	13.58
Tension							
5.36e7	5.06e6	2.37e3	430.36	848.34	14.25	1653.85	27.51
Torsion							
10617.42	561(N-mm)	1.36e4	119.26(N-mm)	1262.70	55.37(N-mm)	61.16	0.53(N-mm)

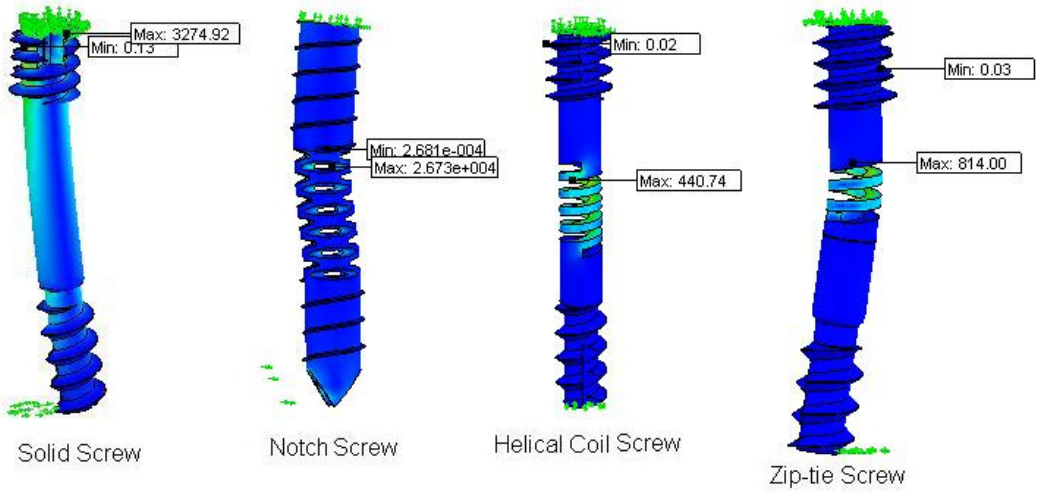

Figure 43: Resulting von Mises stress after 2.5 mm of bending of the different designs. The notch design shows maximum stress and the helical coil cut design shown the minimum. The zip-tie and helical, both showed smaller stress than the solid screw. The helical coil cut performed better than the zip-tie design. The deformations shown here is about 4 times larger than the true scale deformation

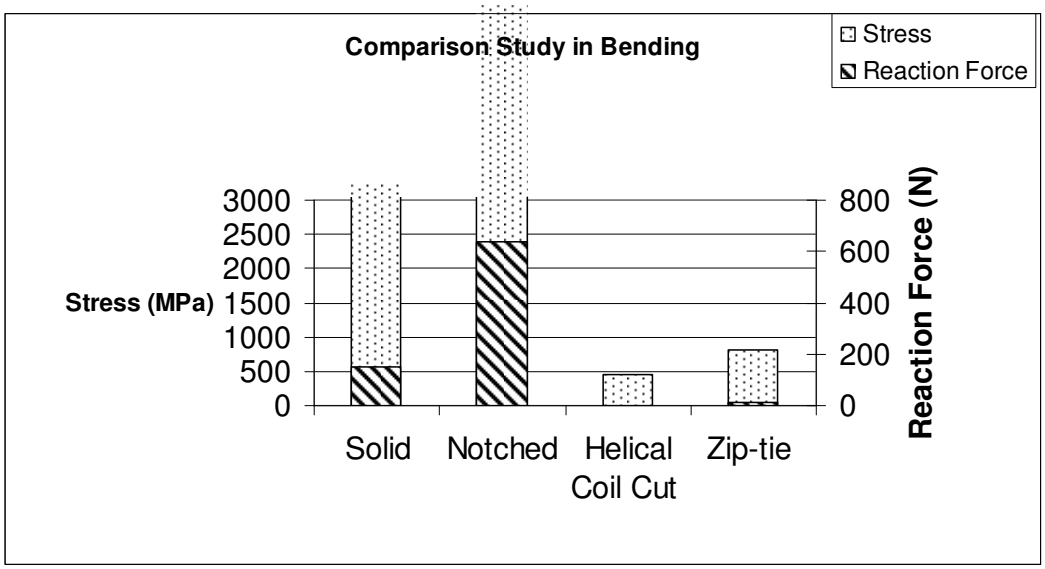

Figure 44: Resulting maximum von Mises stress (primary axis) and reaction force (secondary axis) after 2.5 mm of bending of the different designs. The notch design showed maximum stress and reaction (out of the scale of this graph) and the helical coil cut design shown the minimum. The zip-tie and helical, both show smaller stress than the solid screw. The helical coil cut performed better than the zip-tie design.

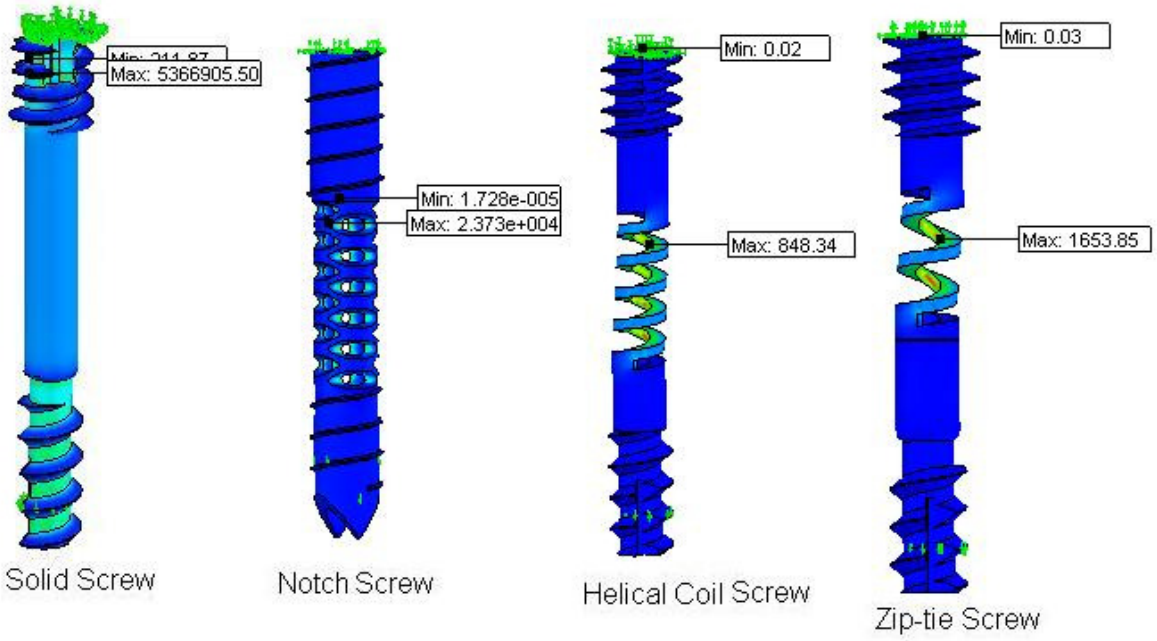

Figure 45: Resulting von Mises stress after 0.3 mm of elongation of the different designs. The solid design shows maximum stress and the helical coil cut design shown the minimum. The zip-tie and helical, both showed smaller stress than the notch screw as well. The helical coil cut performed better than the zip-tie design. The deformations shown here is about 4 times larger than the true scale deformation

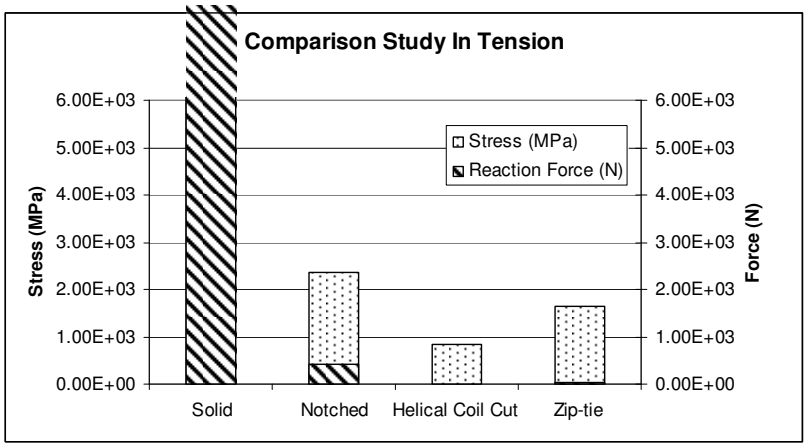

Figure 46: Resulting maximum von Mises stress (primary axis) and reaction force (secondary axis) after 0.3 mm of elongation of the different designs. The solid design shows maximum stress and reaction (out of the scale of this graph) and the helical coil cut design showed the minimum. The zip-tie and helical, both showed smaller stress than the notch screw as well. The helical coil cut performed better than the zip-tie design.

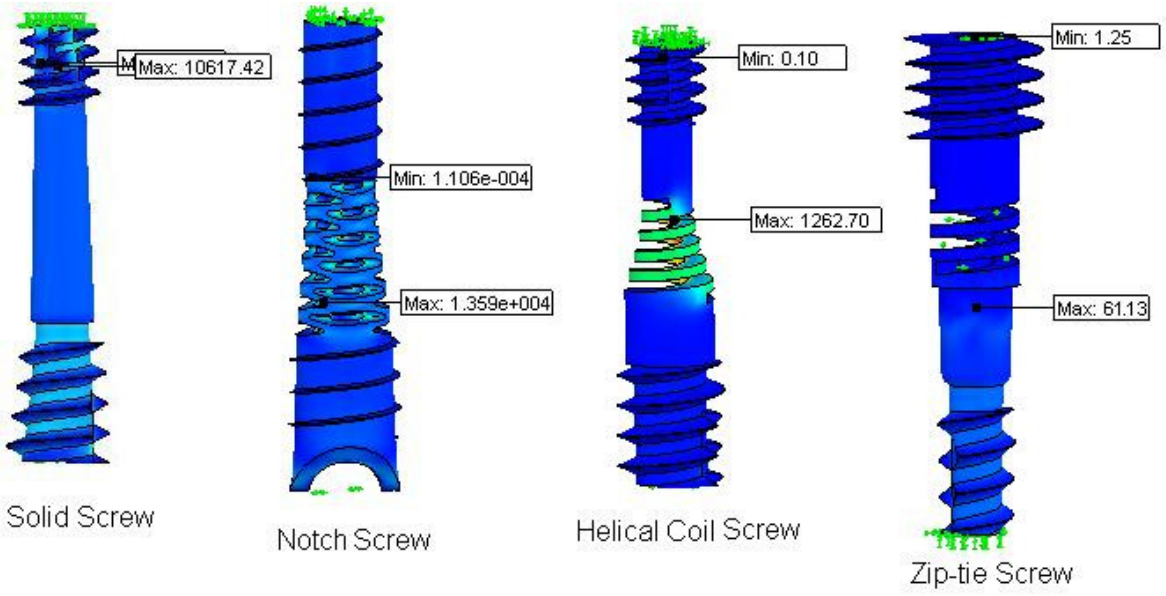

Figure 47: Resulting von Mises stress after 2.5 mm of rotational displacement of the different designs. The notch design showed maximum stress and the zip-tie showed the minimum. The zip-tie and helical, coil cut, both showed smaller stress than the solid screw. The zip-tie performed better than the helical coil cut design. The deformations shown here is about 4 times larger than the true scale deformation.

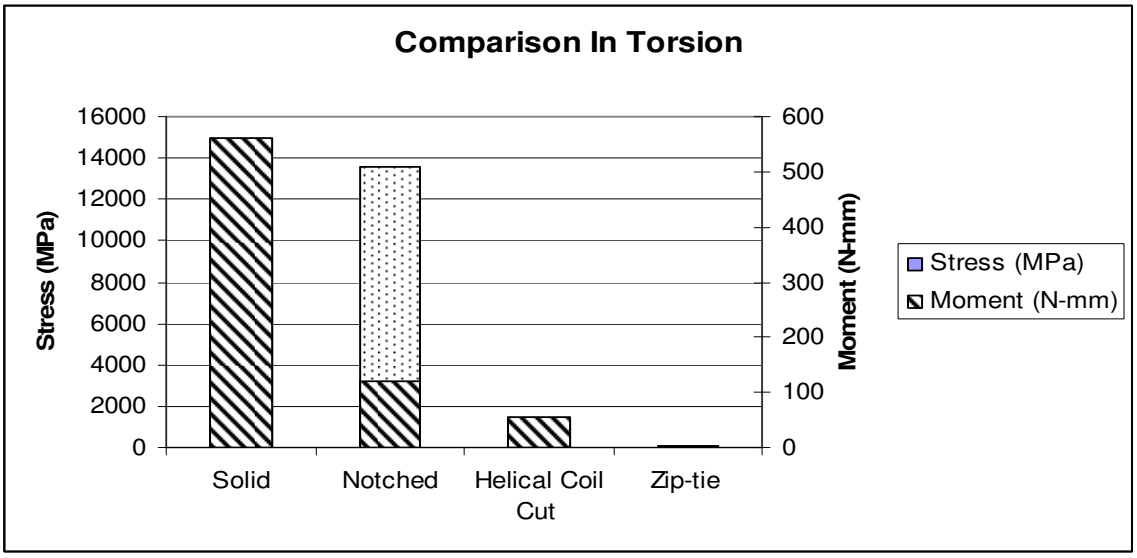

Figure 48: Resulting maximum von Mises stress (primary axis) and reaction force (secondary axis) after 2.5 mm of rotational displacement of the different designs. The notch design showed maximum stress and reaction, and the zip-tie showed the minimum. The zip-tie and helical, coil cut, both showed smaller stress than the solid screw. The zip-tie performed better than the helical coil cut design.

3.4 Fatigue Analysis

When an engineering component is subjected to severe stress, it is prone to failure after a certain number of cycles. When the results of this test from a number of different stress levels are plotted on a logarithmic scale, the resulting curve is called the stress – life curve or S-N curve (Dowling 1999). It is used to determine the failure criteria of an engineering design.

In this study, conducting such a test was out of the scope of the study, and hence some general assumptions were made to calculate the number of cycles to failure for the proposed designs. The resulting stresses from simulation were used for a simplified fatigue analysis using the following equations:

$$\sigma_a = \frac{\sigma_{\max} - \sigma_{\min}}{2} \quad \text{.....(4)}$$

$$\sigma_{a=} = \sigma_f^{'} \left(2N_f\right)^b \quad \text{.....(5)}$$

In equation (4), σ_a is the stress amplitude and in equation (5) N_f is number of cycles to failure, $\sigma_f^{'}$ and *b* are constants based on fitting test data for unnotched axial specimens tested under completely reserved loading. The values were obtained from Dowling's "Mechanical Behavior of Materials" (Dowling 1999). For Titanium alloy, Ti-6Al-4V, $\sigma_f^{'}$ is given 2030 MPa and *b* is given -0.104. The or number of cycles to failure was assumed to be 1e7. Form this equation, the maximum stress was calculated to be about 706 MPa.

Three assumptions were made, (1) the design is unnotched, (2) the minimum stress is zero and (3) the wrist will move about 1e7 times in a year. All of these assumptions may not be true in case of the flexible screw. Therefore the answer to the maximum principle stress to failure is not the exact value for the design. However, the stress values were obtained from a computer simulation using numerical techniques which account the exact geometry. Therefore, assuming unnotched design in the calculation of fatigue is an educated guess. The critical assumption is the life of the screw, which was set to about one year and the assumption was that the wrist will move about 1e7 times in a year. If this assumption is not correct, and if the number is larger, the screw may fail within a year. If it is correct, after one year the screw needs to be removed. Therefore, it can be said that none of the designs will be able to withstand the displacement applied in this study. The helical coil cut design will fail under torsion condition and the zip-tie design will fail under bending conditions for the applied displacement used in this study.

In this study, all the analysis was performed assuming the factor of safety to one. This was to find the maximum flexibility possible by the screws. When the factor of safety increases, for example, to 1.5 or 2, which is necessary for any design, the flexibility of the screws will decrease and it will be prone to failure.

3.5 Prototypes of the Designs

The helical coil cut design from design concept 1 was prototyped (Fig. 49) using solid screws. Three different sizes of the Herbert—Whipple Cannulated Bone Screw from Zimmer® (Warsaw, Indiana) were used. The material was Ti-6Al-4V, the same Titanium

alloy used for simulations of the design. The Helical Products Company Inc (Santa Maria, California) made the flexure cut in the screws.

This prototype was made to test insertion and flexibility in the wrist using a cadaver specimen. One of the screws was inserted into cadaver wrist bones but due to the instability of the flexible section, it was difficult to place the screw within the bones. Based on this study, modification was made to the guide pin to help keep the flexible section rigid during insertion.

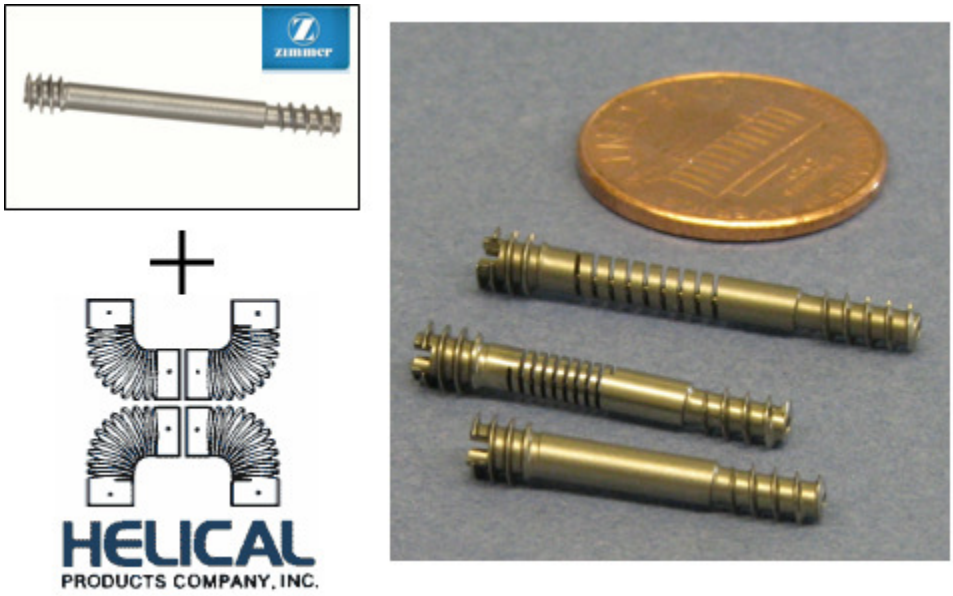

Figure 49: Prototyped screw of the helical coil cut design using solid screw (top left) from Zimmer®. The helical coil cut was made from Helical Products Company Inc.

Design 2, the zip-tie design was also prototyped using rapid prototyping machine (Fig. 50). The technique used in the rapid prototyping machine is stereolithography apparatus or SLA. This is a unique rapid manufacturing and rapid prototyping technology for producing parts with high accuracy (typically about 0.1 mm / 0.004 inches) and good

surface finish. As shown in the picture, the part built in the rapid prototyping machine is six times bigger than the original dimension. The purpose of this prototype was to investigate the assembly and flexibility of the design. After the prototype was made it was understood that assembling the screws by inserting the trailing screw into the leading screw is somewhat difficult and the design need modification in that area.

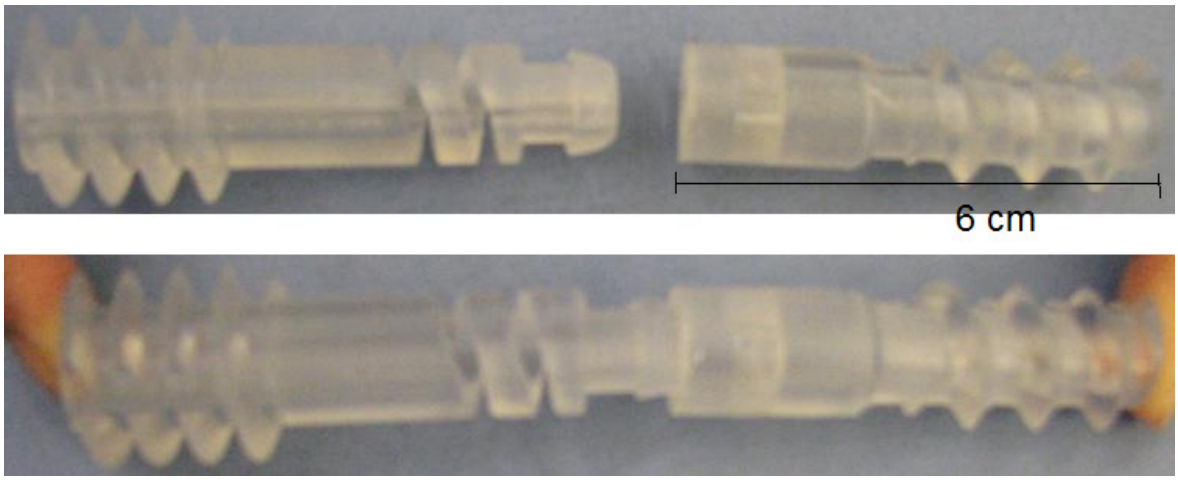

Figure 50: Prototyped Zip-tie model made from a rapid prototyping machine using SLA technique. The top image shows the two parts before insertion and the bottom image shows how they would insert for assembly. Assembly was not possible just by applying force with the hand. These parts are six times larger that actual size

CHAPTER 4 DISCUSSION AND CONCLUSION

4.1 Comparison of Different Designs

In this study a total of five different design ideas were proposed in replacement to the state of the art, the solid screws. Except the notched screw, none of them have any disadvantages in comparison to current products in the market. However, every design has its won challenges compare to another design. In other worlds none of the design met all the design criteria. Also they did not performed to be safe in FEA and almost all of them are challenging in terms of manufacturing.

As it was mentioned before, the spring or cable designs would have adverse effects when they are used in vivo, if they are produced by welding the materials. The helical coil cut design does offer a solution to this problem since it can be manufactured from a single tube. However, all the concepts from Design 1 fail to address the independent rotation ability of the leading and trailing edge. Even if the helical coil cut design can rotate moderately, the resulting stress on the bones is very high.

These were addressed in the second design, Design 2. It permits about 30º of rotation between the leading and trailing edge. It also does not cause any stress to the bones or to the screw itself. However, this design does not have as much bending ability as

the helical coil cut design since there is not much room to cut a long coil to create a spring type mechanism in the tube.

In comparison to the helical coil cut design and the zip-tie design, the helical coil cut is relatively easier to manufacture, no assembly is required after making the screw and above all, it performs the best in bending condition. On the other hand the zip-tie design is relatively difficult to manufacture, requires assembly to make the screw and, in terms of performance, it really can not bend as much as the helical coil cut design. However, this design can give the full range of rotational displacement that is required by the bones. Thus, more development in prototyping and experimentation are necessary in order to come to any resolution with this specific injury.

Finally, even if we assume that the manufacturing issue was overcome, certain problems would still remain. The most important one is the fatigue life. Originally the screw was thought to be within the bones after the surgery for more than a year. This is to avoid multiple surgeries in the wrist. But none of the design can withstand the forces it may observe in vivo for a reasonably long period of time.

4.2. Scientific Contributions and Deliverable:

It is true that none of the design meets all the requirements. However, the zip-tie and the helical coil cut designs have some promises in terms of their functionality. Therefore it can be said that the invented flexible bone screw implant is unique with respect to all other technologies that are being used today for this specific injuty. It also can be used to couple other small bones in the wrist as above (specifically the luno-

triquetral joint). The distal radioulna joint (DRUJ) is an additional site where this technology could be useful. This type of flexible co-aption provided by our screw system could allow healing of TFCC (triangular fibro-cartilage complex) tears without the rigid fixation (pins) used now. The acromio-clavicular joint (AC Joint) in the shoulder is a frequent site of sprains. Although surgical stabilization is seldom necessary, this screw system might offer the perfect solution. There may be a role for a similar system in the ankle to secure the fibula to the tibia in severe ankle sprains in which the syndesmotic ligament is disrupted. Currently, this is treated with a rigid screw that loosens over time or is removed at a later surgery. SLAC or scapholunate instability is considered to be an unsolved problem in orthopedics. The goal was to deliver a solution to this problem.

There are many more steps, such as cadaver study to study movement inside the bones, biocompatibility, and modification in terms of insertion that need to be investigated more in detail before the implant can be implanted in patients. As it was hypothesized that the screw might be useful for some other bone joints, it can also be investigated to maximize the use of the flexible screw.

4.3 Conclusion:

Proposed technique involves design of a flexible structure/section in a bone screw implant to provide a relative motion between the scaphoid and lunate bones. Current technology uses solid screws of different sizes and configuration. As a result the bones are not free to move. The main advantage of the invented system is that it allows for more

normal wrist biomechanics and avoids the potential bone damage associated with the placement of a rigid device between two moving bones.

The use of a flexible design to make orthopedic screws is unique with respect to all other technologies that are being used today. Current technologies like Herbert Screw, TwinFix Cannulated Compression Screw, or Acutrak Screw System, as mentioned before, fuses the bones together in order to hold them in compression. The SLIC screw has a flexible joint between the screw halves but it is not available in the market.

Every design has some advantages and disadvantages and some challenges to overcome. For all of them, one of these challenges was the manufacturing and its cost to produce such a fine product to complete the study. Before the screw can be used for patients, there are many steps that need to be done. However, it can be said that the novel flexible bone screw implant can provide a technique to obtain secure and biomechanically sound coupling between the dissociated scaphoid and lunate bones in the wrist

Literature Cited

"Acumed - Acutrak 2® Standard" http://www.acumed.net/product/19 (accessed Jan. 11th 2008)

Aviles AJ, Lee SK, Hausman MR. "*Arthroscopicreduction-association of the scapholunate*." Arthroscopy 23(2007) pages105.e1-105.e5

Baratz, Mark, Melvin P. Rosenwasser, Brian D. Adams, and Scott Kozin. *Wrist Surgery.* New York: Thieme, 2006, page 100-112

Berger, Richard A. "The gross and histologic anatomy of the scapholunate interosseous ligament." *J Hand Surg* 21, no. A (1996):170-178

Bowlin, Gary L. *Biomaterials (EGRB 427).* Lecture, Virginia Commonwealth University, Richmond, VA. Fall 2006

Budoff, Jeffrey E. MD. Treatment of Acute Lunate and Perilunate Dislocations. *J Hand Surg.*33 no A (2008):1424 – 1432

Chabas, Jean-François, André Gay, David Valenti, et al. Results of the Modified Brunelli Tenodesis for Treatment of Scapholunate Instability: A Retrospective Study of 19 Patients. *J of Hand Surg*. 33 no 9(2008):1469-77

Cooney,William P. *The Wrist: Diagnosis and Operative Treatment.* Ronald L. Linscheid, and James H. Dobyns. Philadelphia: Mosby, 1998, Chap 4, p63-93 and chap. 21, p501-526

Craigen. M.A. and J.K. Stanley, Wrist Kinematics. Row, column or both? *J of Hand Surg Br.*, 20 (1995): 165-170

Danikas, Dimitrios. "Scapholunate Advanced Collapse." e-medicine. 07 May 2005. WebMD <http://www.emedicine.com/orthoped/topic553.htm#section~author_information>(accessed 2 Apr 2007)

Dowling, Norman E. *Mechanical Behavior of Materials*. New Jersey: Prentice Hall, 1999, page 395

Doyle, James R , and Michael J Botte. *Surgical Anatomy of the Hand and Upper Extremity*. Philadelphia: Lippincott Williams & Wilkins, 2003, page 501

Franssen, "Kirschner wire." November 16th, 2008 .http://www.kirschnerwire.com/Index.html (accessed Nov. 25th, 2008).

Garcia-Elias, Marc. *Wrist instability* Ueli Büchler. London: Mosby, 1996, page 9

Gupta. Ajay, and Nawal M. Al-Moosawi. Lunate morphology. *Journal of Biomechanics* 35 (2002): 1451–1457

"Herbert/Whipple Cannulated Screws." http://catalog.zimmer.com/content/zpc/products/300/325/348/EL206/0531.html (accessed Jan. 11th 2008)

Harvey, Edward J., Richard A. Berger, Lee Osterman, et al. Bone–Tissue–Bone Repairs for Scapholunate Dissociation. *J Hand Surg*. 32 no A (2007): 256–64

Heinzelmann, Andrew D., Graeme Archer, and Randy R. Bindra. "Anthropometry of the Human Scaphoid" *J Hand Surg*. 32 no A (2007):1005-08

"Helical" http://www.heli-cal.com/cm/Home.html (accessed May 11th 2008)

Jaruga, Maciej M., Wladyslaw W Manikowski, Maria M. Jaruga, Piotr P. Czarnecki. "Rehabilitation after operative treatment of carpal instability." *Ortop Traumatol Rehabil.* 8(2006): 282-7.

Kuo, Christina E. and Scott W. Wolfe. "Scapholunate Instability – Current concepts in Diagnosis and Management." *J Hand Surg*. 33 no A (2008):998-1013

Larsen, Claus F. *Wrist instability*. Ueli Büchler. London: Mosby, 1996, page 97

Lichtman, David M. *The Wrist and its Disorder*. Philadelphia: W.B. Saunders Company, 1988, Chap 2, 4, p14-45

Moran, Steven L., William P. Cooney, Richard A. Berger, and Justin Strickland. "Capsulodesis for the treatment of chronic scapholunate instability." *J Hand Surg.* 30 no A (2005):16–23

"Orthosurgical Implants" http://www.orthosurgical.com/pdfs/HBS_STANDAR.pdf (accessed Aug. 18th 2008)

Rosenwasser, Melvin P, and Robert J. Strauch and Kenji C. Miyasajsa. "The RASL procedure: reduction and association of the scaphoid and lunate using the Herbert screw." *Tech Hand Up Extrem Surg* 1 no 4 (1997):263-72

Shepherd D.E.T., and Johnstone A.J. "Design Consideration for a Wrist Implant." *Medical Engineering & Physics* 24 (2002): 641-650

Short, Walter H., Frederic W. Werner, Jason K. Green and Shunji Masaoka. "Biomechanical evaluation of ligamentous stabilizers of the scaphoid and lunate." *J Hand Surg.* 27 no A (2002):991-1002

Short, Walter H., Frederick W. Werner, and Levi G. Sutton. "Treatment of Scapholunate Dissociation With a Bioresorbable Polymer Plate: A Biomechanical Study" *J Hand Surg*. 33 no A (2008):643 – 649

Short, Walter H., Frederic W. Werner, Jason K. Green and Shunji Masaoka. "Biomechanical evaluation of ligamentous stabilizers of the scaphoid and lunate: Part II." *J Hand Surg.* 30 no A (2005):24-34

Short, Walter H., Frederic W. Werner, Jason K. Green and Shunji Masaoka. "Biomechanical evaluation of ligamentous stabilizers of the scaphoid and lunate: Part III." *J Hand Surg.* 32 no A (2007):297e1-297e18

Short, Walter H., Frederic W. Werner, Maria D. Fortino and Kenneth A. Mann. "Analysis of the Kinematics of the Scaphoid and Lunate in the Intact Wrist joint" *Biomechanics of the Hand and Wrist* 13 no 1 (1997):93-98

Spitalny, Douglas A. "Bioabsorbable Implants" *Clin Podiatr Med Surg* 23 (2006) 673–694

"Stryker" http://www.europe.stryker.com/leibinger.com (accessed Jan. 11th 2008)

Sucec, Matthew C., and Thomas C. Tuller, "Bone Connector with Pivotable Joint," *U.S. Patent* 2006/0271054 A1, Nov. 30, 2006

Taleisnik, Julio. *The Wrist* . New York : Churchill Livingstone, 1985, Chap 1, p3-25
Walsh, John J., Richard A. Berger, and William P. Cooney. "Current Status of Scapholunate Interosseous Ligament Injuries." *Journal of the American Academy of Orthopaedic Surgeons*. 10 (2002):32-42

Weiss, Arnold-Peter C. "Scapholunate ligament reconstruction using a bone-retinaculum-bone autograft" *J Hand Surg*. 23, no 2(1998), p 205-215

Werner, Fredrick W., Walter H. Short and Jason K. Green. Changes in Patterns of Scaphoid and Lunate Motion During Functional Arcs of Wrist Motion Induced by Ligament Division. *J Hand Surg*. 30 no A (2005):1156-1160

Wolfe, Scott W. "Scapholunate Instability." *Journal of the American Society for Surgery of the Hand*. 1 no (2001)

"Zimmer - Trauma - Zimmer Herbert™ Cannulated Bone Screw" http://www.zimmer.com/z/ctl/op/global/action/1/id/9214/template/MP/prcat/M7/prod/y (accessed Jan. 11th 2008)

LIST OF ABBREVEATION

CT	Computer Tomography
D	Dorsal
DISI	Dorsal Intercalated Segment Instability
FEA	Finite Element Analysis
HBS	Herbert Bone Screw
L	Lunate
lb	Pound
mm	Millimeter
OCD	Osteochondritis Dissecans
P	Palmar
Px	Proximal
RASL	Reapproximation of Scaphoid and Lunate
S	Scaphoid
SLAC	Scapholunate Advanced Collapse
SLI	Scapholunate Interosseous
voM	von Mises Stress

APPENDIX A: Technical Drawing of the Notch Design

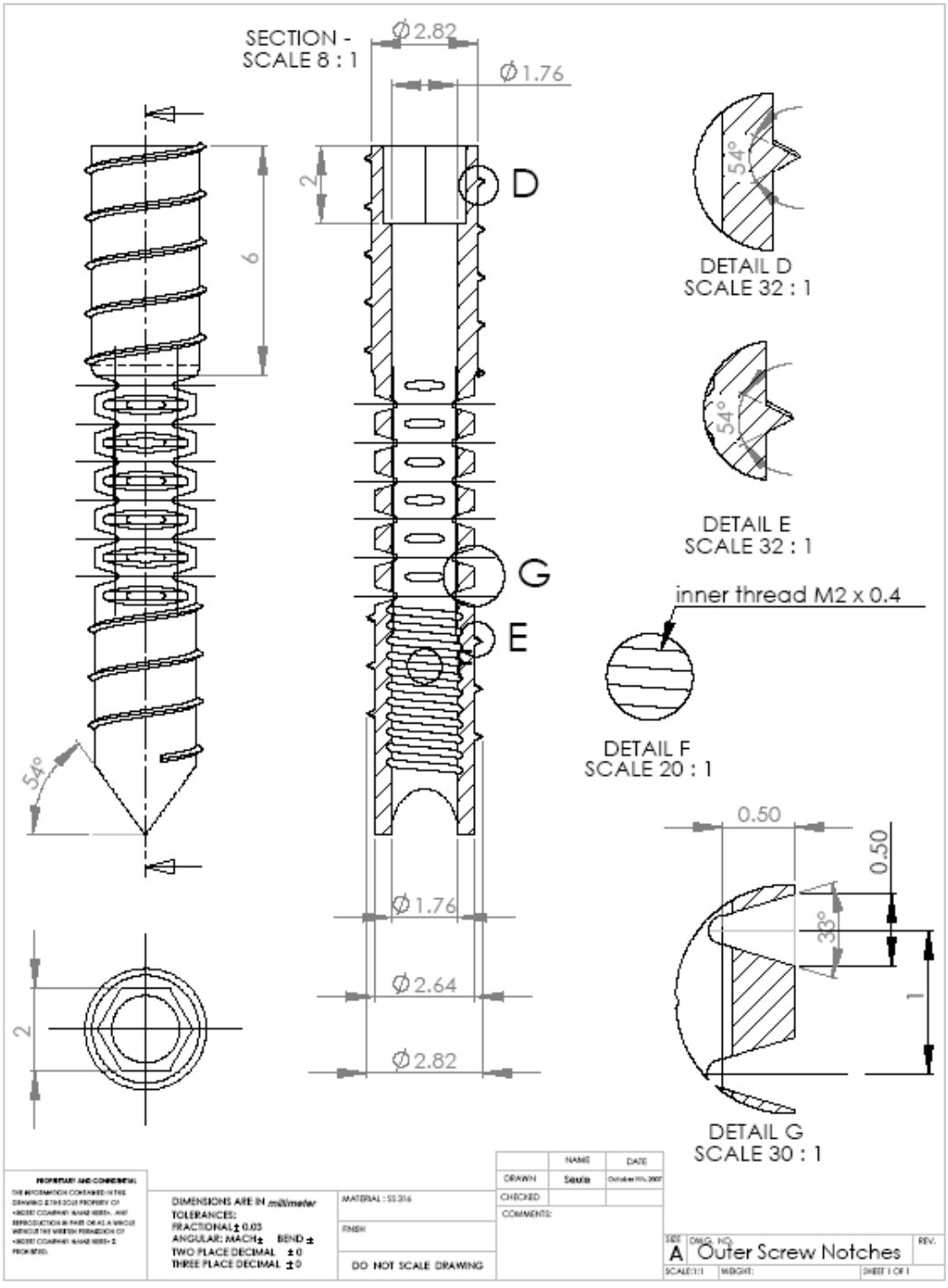

APPENDIX B: Technical Drawing of a Helical Coil Cut Screw Design

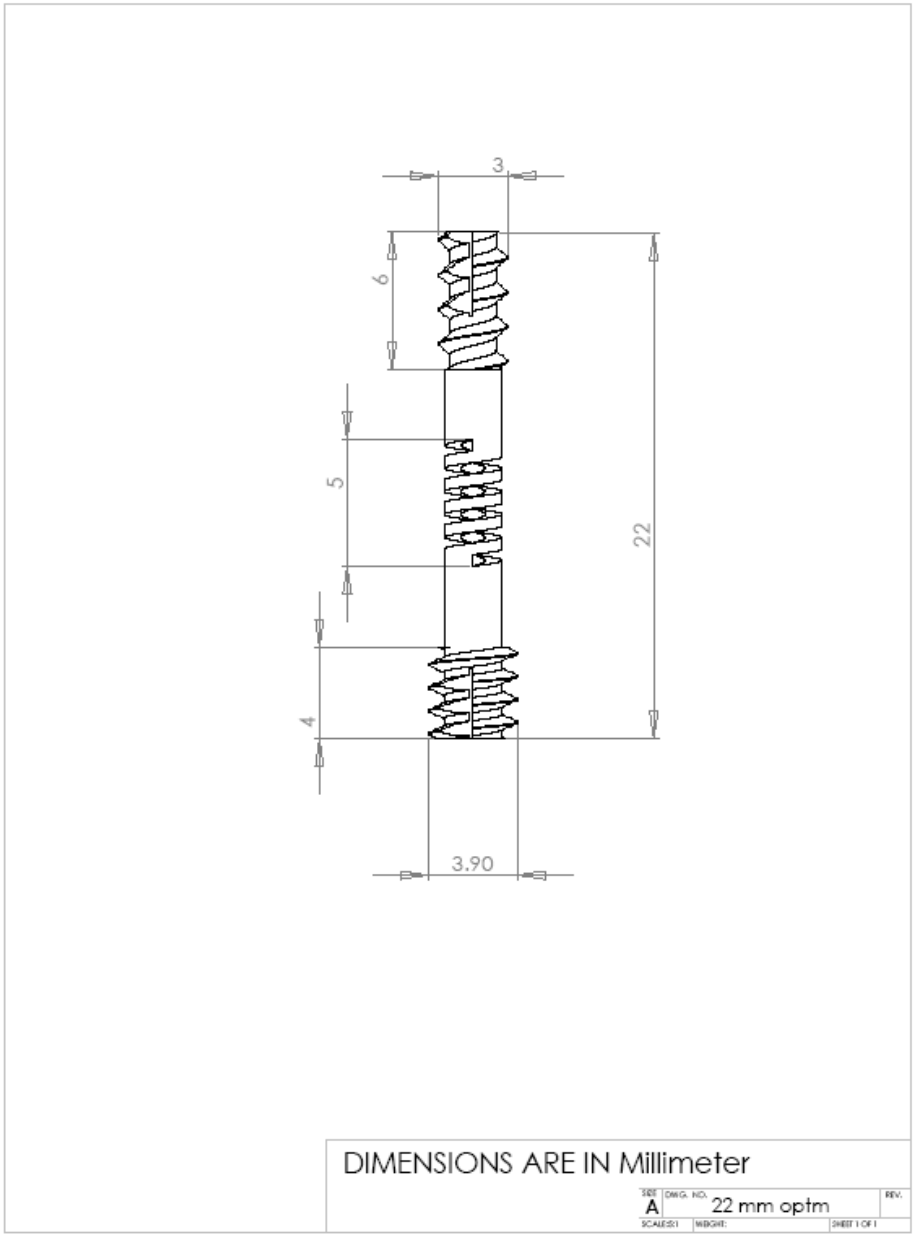

Appendix C1: Technical Drawings of the Leading Screw (Design 2)

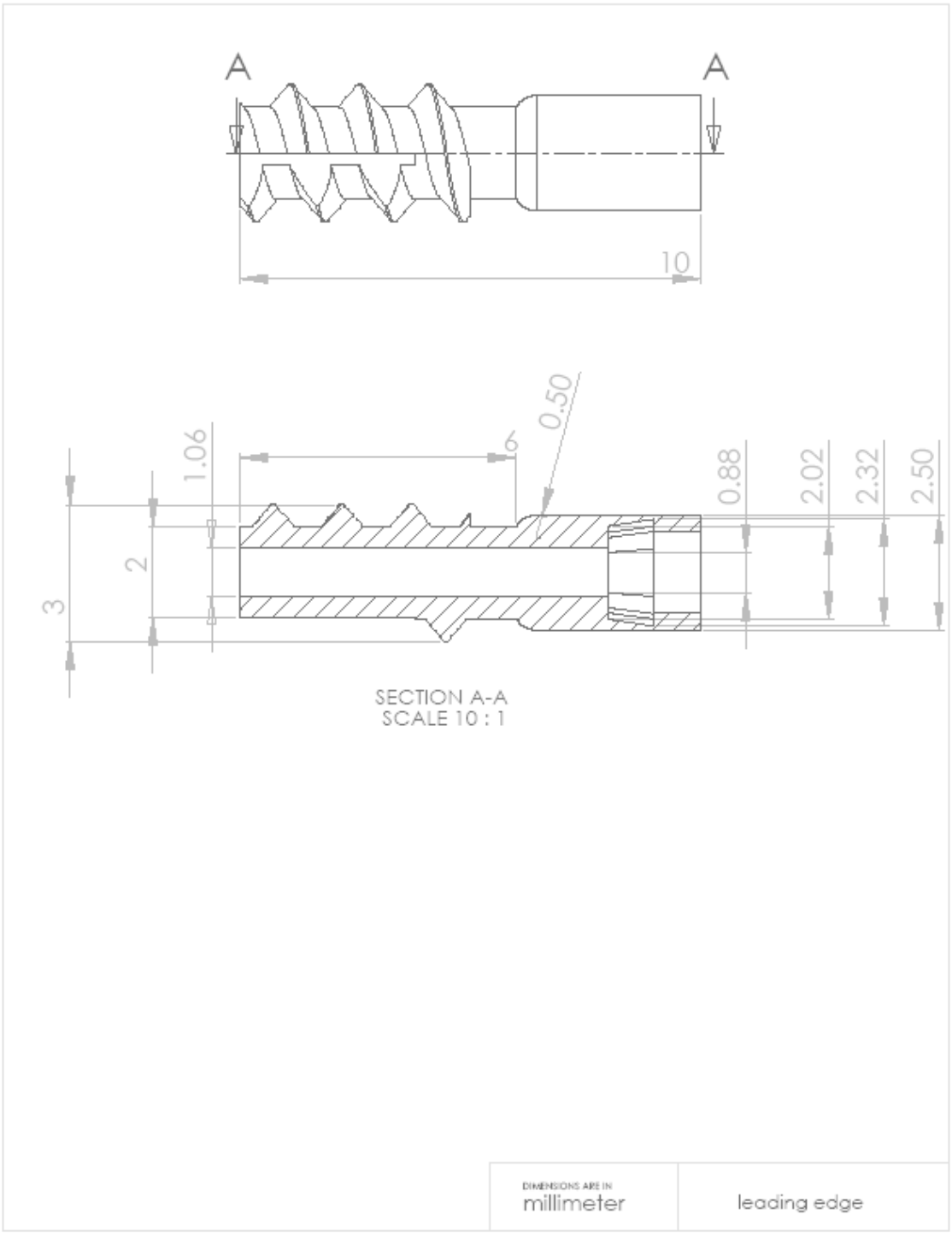

Appendix C2: Technical Drawings of the Trailing Screw (Design 2)